

Evidence of Exponential Decay Emission in the *Swift* Gamma-ray Bursts

T. Sakamoto^{1,2}, J. E. Hill^{1,3,4}, R. Yamazaki⁵, L. Angelini¹, H. A. Krimm^{1,3,4}, G. Sato^{1,6},
S. Swindell⁷, K. Takami⁵, J. P. Osborne⁸

ABSTRACT

We present a systematic study of the steep decay emission from gamma-ray bursts (GRBs) observed by the *Swift* X-Ray Telescope (XRT). In contrast to the analysis described in recent literature, we produce composite Burst Alert Telescope (BAT) and XRT light curves by extrapolating the XRT data (2–10 keV) into the BAT energy range (15–25 keV) rather than extrapolating the BAT data into the XRT energy band (0.3–10 keV). Based on the fits to the composite light curves, we have confirmed the existence of an exponential decay component which smoothly connects the BAT prompt data to the XRT steep decay for several GRBs. We also find that the XRT steep decay for some of the bursts can be well fit by a combination of a power-law with an exponential decay model. We discuss this exponential component within the frame work of both the internal and the external shock model.

Subject headings: Gamma-ray Burst

¹NASA Goddard Space Flight Center, Greenbelt, MD 20771

²Oak Ridge Associated Universities, P.O. Box 117, Oak Ridge, Tennessee 37831-0117

³CRESST NASA Goddard Space Flight Center, Greenbelt, MD 20771

⁴Universities Space Research Association, 10211 Wincopin Circle, Suite 500, Columbia, MD 21044-3432

⁵Department of Physics, Hiroshima University, Higashi-Hiroshima, Hiroshima, 739-8526, Japan

⁶Institute of Space and Astronautical Science, JAXA, Kanagawa 229-8510, Japan

⁷Department of Physics, North Carolina Agricultural and Technical State University, 1601 East Market Street, Greensboro, North Carolina 27411

⁸Department of Physics and Astronomy, University of Leicester, LE1, 7RH, UK

1. Introduction

The transition between the gamma-ray burst (GRB) prompt emission and afterglow emission has generated great interest within the scientific community. It is generally accepted that the GRB prompt emission is due to internal shocks originating from the collision of faster and slower moving shells, whereas, the afterglow is believed to originate from an external shock resulting from the relativistic fireball colliding with a circum-burst medium (Rees & Mészáros 1994; Sari & Piran 1997; Mészáros & Rees 1997). During the GRB episode there should be a transition from one phase to the other, however, it is still not well understood as to when this transition occurs. The Burst and Transient Source Experiment (BATSE) observation of GRB 980923 showed long lasting tail emission, ~ 400 s, which is best described by a power-law temporal decay (Giblin et al. 1999). Based on the spectral and temporal characteristics of this burst, Giblin et al. (1999) concluded that the tail emission was a part of the afterglow emission, thus, the external shock could be generated during the prompt γ -ray phase. Giblin et al. (2002) performed a systematic study of the prompt tail emission using 40 GRBs observed by BATSE. They found that the temporal decays are best described by a power-law with a decay index of -2 rather than an exponential. There are several other analysis of BATSE data which reach the same conclusion (e.g., Ryde & Svensson 2002). According to the BeppoSAX observations, the late time afterglow smoothly connects with the prompt emission if the onset time of the light curve is defined as the start time of the last pulse observed in the Wide Field Camera (2–30 keV) (e.g., Pian et al. 2001; Piro et al. 2005). These observations support the idea that the late X-ray spike represents the onset of the afterglow. However, the delay of a few hours to a few days before the narrow field X-ray instrument is pointed to the GRB position, weakens the discussion concerning the transition from the prompt emission to the afterglow.

As a result of the revolutionary features of *Swift* (Gehrels et al. 2004), our understanding of the X-ray properties of GRBs has been improved dramatically. With the combination of the accurate on-board calculation of the GRB position by the Burst Alert Telescope (BAT:15–150 keV; Barthelmy et al. 2005) and the fast slewing capability of the spacecraft, *Swift* can begin a highly sensitive X-ray observation with the X-Ray Telescope (XRT:0.2–10 keV; Burrows et al. 2005) within a few tens of seconds to a few hundred seconds after the burst trigger. According to the XRT observations, the X-ray properties of the GRB emission have very complex features (Nousek et al. 2006; Zhang et al. 2006a). One of the most unexpected discoveries by the XRT is the existence of the steep decay component during the initial phase of the X-ray light curve. The origin of this steep decay component is generally considered to be a result of the delayed prompt emission from different viewing latitudes of the jet, the so called “curvature effect” (e.g. Fenimore et al. 1996; Kumar & Panaitescu 2000; Zhang et al. 2006a). Tagliaferri et al. (2005) and Barthelmy et al. (2006) investigated the steep decay

component with the composite BAT and XRT light curves for several GRBs. To generate the composite light curve, both papers performed an extrapolation of the BAT mask-weighted (background subtracted) light curve into the XRT 0.2–10 keV energy band using a best-fit power-law photon index. The authors found that GRB 050126 and GRB 050219A do not show continuous emission from the BAT to the XRT light curve, however, GRB 050315 and GRB 050319 do display a smooth continuation from the BAT to the XRT light curve. O’Brien et al. (2006) performed a systematic study of the early X-ray emission using a sample of 40 *Swift* GRBs. They constructed a composite BAT and XRT light curve in the 0.3–10 keV band. In order to extrapolate the BAT data points, the BAT mask-weighted count rate was converted to flux in the 0.3–10 keV band using the mean of the best-fit photon indices obtained from a simple power-law fit to both the BAT and the XRT spectrum. The authors found that a fit of the 40 superimposed GRB light curves in the 0.3–10 keV band could be described by an exponential decay followed by a power-law decay. Willingale et al. (2007) investigated the X-ray emission including the late time light curve data. They found that the X-ray light curve data can be modeled with the superposition of an early (“prompt”) and a late time (“afterglow”) component.

In this paper, we describe the analysis of the tail emission using an alternative approach. We generate the composite BAT and XRT light curve in the 15–25 keV BAT energy band by extrapolating the 2–10 keV XRT count rate into the 15–25 keV band. Either approach, extrapolating the BAT count rate down to the XRT band (hereafter BAT-to-XRT extrapolation) or extrapolating the XRT count rate up to the BAT band (hereafter XRT-to-BAT extrapolation), can encounter similar systematic problems. Most of the GRB prompt emission spectra is well fit by the Band function (Band et al. 1993) with a low-energy and a high-energy photon index of ~ 1 and ~ 2.3 , respectively (e.g. Sakamoto et al. 2005; Kaneko et al. 2006). However, it is a well known characteristic that the peak energy of the spectrum, E_{peak} , not only evolves during the burst (e.g., Lloyd-Ronning and Petrosian 2002; Frontera et al. 1999) but also changes from burst-to-burst (e.g., Sakamoto et al. 2005). Here, we discuss the issues with regard to both types of extrapolation by considering five cases depending on the value of E_{peak} (shown in figure 1 left is the BAT-to-XRT extrapolation and right is the XRT-to-BAT extrapolation). If we consider the energy bands of the BAT (15–150 keV) and the XRT (0.3–10 keV), the five cases are defined by: 1) $E_{\text{peak}} > 150$ keV, 2) $15 \text{ keV} < E_{\text{peak}} < 150 \text{ keV}$, 3) $10 \text{ keV} < E_{\text{peak}} < 15 \text{ keV}$, 4) $0.3 \text{ keV} < E_{\text{peak}} < 10 \text{ keV}$, and 5) $E_{\text{peak}} < 0.3 \text{ keV}$. For cases 1 and 5, both the BAT-to-XRT and the XRT-to-BAT extrapolations should provide the correct flux because the photon index of the extrapolated energy band is the same as the observed energy band (“1” and “5” of the left and the right panels of figure 1). For cases 3 and 4, the BAT-to-XRT extrapolation would over estimate the flux in the XRT energy band, since the photon index in the observed energy band is

steeper than that of the extrapolated energy band (“3” and “4” of the left panel of figure 1). Similarly, for case 2 and 3, the XRT-to-BAT extrapolation would over estimate the flux in the BAT energy band, because the photon index in the observed energy band is shallower than that of the extrapolated energy band (“2” and “3” of the right panel of figure 1). For case 2, using the BAT-to-XRT extrapolation (“2” of the left panel of figure 1), and for case 4, using the XRT-to-BAT extrapolation (“4” of the right panel of figure 1), the flux would be overestimated in the XRT and the BAT energy band respectively, because the simple power-law fit is a tangential line to the curved spectrum as a result of the narrow energy bands of the BAT and the XRT (e.g. Sakamoto et al. in preparation).

To date, most of the BAT and XRT composite light curves in the literature have been produced from a BAT-to-XRT extrapolation. However, we believe that the XRT-to-BAT extrapolation described here may minimize the systematic errors, especially with respect to investigating GRB tail emission, for the following three reasons. First, we can account for the spectral evolution during the prompt emission if we extract the flux from the time-resolved spectral analysis of the BAT data. As previously mentioned, E_{peak} shifts from hundreds of keV to a few keV during the prompt emission. If in the analysis, one does not account for the spectral evolution during the prompt emission, which is the case for the majority of the published XRT and BAT composite light curves using the BAT-to-XRT extrapolation, the systematic error in the extrapolated flux in the X-ray range could be significant. Second, since the BAT mask-weighted count rate does not correct for the energy dependence of each photon, the count rate of the source in the off-axis direction will be systematically smaller than the on-axis case. This effect becomes an issue when the BAT-to-XRT extrapolation has been performed by converting the BAT mask-weighted count-rate into flux using a fixed photon index obtained from a simple power-law fit. According to the BAT Crab observation, the count rate from the Crab is $\sim 15\%$ smaller in the 45 degree off-axis case. This off-axis effect is correctly taken into account in the BAT energy response matrix, but not in the BAT mask-weighted count rates. Therefore, unless one applies an additional off-axis correction to the BAT mask-weighted count rates, a systematically smaller flux is obtained if the source is in the off-axis direction, which is always the case for the BAT GRB data prior to the spacecraft slewing to the GRB position. Third, according to the GRB synchrotron shock model (Sari et al. 1998), if the observed spectrum has a photon index steeper than 2, and a power-law index of an electron distribution, p , in the range of $2 \leq p < 3$ (where $N(\gamma_e) \propto \gamma_e^{-p}$, and γ_e is the Lorentz factor of the electrons), then the observed frequency should be above the synchrotron critical frequency for electrons with a minimum Lorentz factor (ν_m) in the fast cooling phase or above the cooling frequency (ν_c) in the slow cooling phase. In this case, since there is no characteristic frequency above ν_m (in the fast cooling case) and ν_c (in the slow cooling case), it is reasonable to extrapolate upwards in energy. The electron power-law

index $2 \leq p < 3$ is typical for both the prompt emission (e.g., Kaneko et al. 2006) and the afterglow of GRBs (e.g., Panaitescu & Kumar 2002; Yost et al. 2003). Thus, if we select the burst samples which have an observed photon index steeper than 2 in the XRT data, the systematic error in the XRT-to-BAT extrapolation should be reduced.

Following these arguments, we describe in this paper the XRT-to-BAT extrapolation to investigate the nature of the XRT steep decay component. As we mentioned, in principle the XRT-to-BAT extrapolation has similar issues to the BAT-to-XRT extrapolation. However, for certain bursts the XRT-to-BAT extrapolation could greatly reduce the systematic error. More importantly, a different approach to the analysis may provide an alternate view of the problem.

2. Analysis

X-ray light curves were produced from the XRT data for all *Swift* GRBs detected between June 2005¹ and September 2006. 54 GRBs with an early phase power-law decay index steeper than -2 (t_0 taken as the BAT trigger time) were identified. From the spectral analysis of the X-ray data from these bursts in the 0.3 – 10 keV band, we found that many bursts exhibited a significant difference in the best-fit spectral parameters between the early (< 1000 seconds) data and the later (> 1000 seconds) data. This is likely due to the fact that E_{peak} is moving through XRT energy range early in the observation but one cannot measure this from the XRT data alone because of the narrow energy band (e.g., Butler & Kocevski 2007). To minimize the effects of the spectral evolution and also the absorption, only data above 2 keV was used in these analysis. We further refined the burst sample to those which satisfied the following criteria: 1) Greater than four data bins containing at least 20 counts in the 2–10 keV light curve during the early phase (< 1000 seconds). This criteria reduced the number of bursts in the sample significantly, due to much fewer counts being detected above 2 keV. 2) No more than a single flare present in the early XRT light curve². 3) The joint spectral analysis of the Photon Counting (PC) and Windowed Timing (WT) data must include a photon index of 2 in the 90% confidence interval. 13 GRBs satisfied the screening criteria. Since the 2-10 keV joint spectral fit to the PC and WT data includes a best fit photon index steeper than 2 for all the GRBs in the sample, E_{peak} should be below 2 keV.

¹Following updates to the on-board software which compensate for the uncontrolled temperature due to failure of the cooling control system (Kennea et al. 2005), bright Earth effects and micrometeoroid damage (Hill et al. 2005).

²Bursts exhibiting flares in the BAT were not excluded.

This will reduce the systematic error of the extrapolation because there should be no spectral evolution as a result of the shift of E_{peak} during the burst.

As mentioned in Zhang et al. (2006a), the definition of the offset time (t_0) is critical when performing fits to the early phase light curve. Traditionally, t_0 is defined as the trigger time of the GRB instrument; when the count rate exceeds some background level (rate trigger). However, the definition of the BAT trigger time is different. The BAT trigger time is the start time of the foreground time interval of the image from which the GRB is detected on-board. Thus, to be comparable to a rate trigger time, we define t_0 as the start time of the prompt emission (start time of t_{100} interval) for the whole sample.

2.1. BAT analysis

The BAT analysis was performed using HEASoft version 6.1.1 and CALDB version 2006-05-30. The event-by-event data were used for these analysis. The non-linear energy correction for each event was applied by `bateconvert`. The mask-weighting factors were calculated by `batmaskwtevt` using the on-board position. The detector enable and disable map was created by `bathotpix` combining the enable and disable map generated by the flight software. We created the BAT light curve by `batbinevt` in the full energy range (15-350 keV³) in 4 ms bin except for GRB 051109A (64 ms), GRB 060427 (1 s) and GRB 060923C (64 ms). We used larger binning for these three GRBs because of the low signal-to-noise ratio of the emission. The duration and the time intervals based on the Bayesian Block algorithm (Scargle 1998) were calculated by `battblocks`. The spectrum of each time interval was extracted by `batbinevt`. The energy response file was created by `batdrngen`. If the time interval was during the spacecraft slew, we updated the keywords in the spectral file related to the energy response process by `batupdatephakw` and then created the energy response file for the time interval by `batdrngen`. We applied systematic error vectors to the spectrum using `batphasyserr` prior to doing the spectral analysis. The spectral analysis was performed using Xspec 11.3.2.

The energy flux in the 15–25 keV band was calculated for each time interval directly from the spectral fitting process. The spectra from each time interval were fitted with a simple power-law model. According to the BAT GRB catalog (Angelini et al. in preparation), the detection threshold of the BAT in the 15–25 keV band is $\sim 10^{-9}$ ergs cm⁻² s⁻¹. Based on this result, the 15–25 keV flux was treated as an upper limit when the calculated 15–

³The coded mask is transparent to photons above 150 keV. Thus, photons above 150 keV are treated as background in the mask-weighted method. The effective upper boundary is ~ 150 keV.

25 keV flux was less than 10^{-9} ergs cm $^{-2}$ s $^{-1}$. The upper limit was estimated from using the event-by-event data from the Crab nebula on-axis observation collected on 2005 March 24 (observation ID: 00050100016). According to this observation, the BAT can detect the Crab nebula in the 15–25 keV band at 5σ in a one second exposure. Assuming that the BAT sensitivity scales as the square-root of the exposure time (Markwardt et al. 2005) and a canonical Crab flux of 5.3×10^{-9} ergs cm $^{-2}$ s $^{-1}$ in the 15–25 keV band, we calculated the BAT 5σ upper limit in the 15–25 keV band from the following equation,

$$F(15 - 25\text{keV})_{5\sigma} = \frac{5.3 \times 10^{-9}}{f_{pcode}} t_{exp}^{-0.5} \text{ (ergs cm}^{-2} \text{ s}^{-1}\text{)}. \quad (1)$$

Here t_{exp} is the exposure time and f_{pcode} is the partial coded fraction. Since our estimation of the 5σ upper limit is based on the on-axis Crab observation, f_{pcode} will correct for a source observed in the off-axis direction.

For the time-averaged spectral analysis, we use the time interval from the emission start time to the emission end time (t_{100} interval). When the spacecraft slew occurred during the time interval, we created the response matrices for each five second period, taking into account the position of the GRB in detector coordinates. We then weighted these response matrices by the five second count rates and created the averaged response matrices. Since the spacecraft slews about one degree per one second in response to a GRB trigger, we choose five second intervals to calculate the energy response for every five degrees.

2.2. XRT analysis

The 13 bursts meeting the criteria outlined in section 2 were processed using the HEASoft tools version 6.1.1 including version 2.5a of the *Swift* software. The level 2 cleaned event files were produced from the `xrtpipeline` task (version 10.4) using the standard screening criteria. Version 8 of the response matrices in CALDB and the corresponding ancillary response produced from `xrtmkarf` were used. The standard grades (Burrows et al. 2005) were used in the analysis; grades 0-2 and 0-12 for WT and PC mode, respectively.

Both WT and PC mode data (Hill et al. 2004, 2005) from the first observation segment (000) were analyzed. The source and background extraction regions were nominally a 40-pixel square and an annulus with a 3 pixel inner radius and 25 pixel outer radius for WT and for PC mode, respectively. The extraction regions were modified for the piled-up cases in WT mode in accordance with Romano et al. (2006), eliminating an inner square centered on the source. It is well documented that pile-up in PC mode causes a redistribution of single pixel events to higher grades (Vaughan et al. 2006). In order to account for pile-up

in PC mode, the grade distributions were analyzed for each burst during periods where the count-rate exceeded 0.5 counts/sec. For each burst, the percentage of single pixel events were plotted versus the radius of the center of the annulus for increasing radii (0–8 pixels). The annulus with smallest radius at which the percentage of single pixel events became constant was used for the PC mode analysis. Nominally, for a spectrum where the average energy is 1.5 keV, 78% of the events will be single pixel events (Moretti et al. 2004).

The hardness ratio ((2.0–10.0)keV/(0.5–2.0) keV) was examined for each burst to ensure that there was no significant spectral evolution. An exposure map was created from `xrtepomap` to correct for the dead columns and hot pixels. `xrtmkarf` was used to create the ancillary response files. This includes corrections for losses in the wings of the point spread function and the center of the annulus, for the exposure and for vignetting.

The spectrum file was binned with a minimum of 20 counts/bin in order for χ^2 statistics to be valid for the spectral fitting. Xspec version 11.3.2 was used to perform a joint spectral fit of the WT and PC data from 2–10 keV using a simple power law model. The 15–25 keV normalization obtained from the *peppwrlw* model was used to extrapolate the XRT count rate into flux in the BAT 15–25 keV energy range. Only light curve bins with greater than 90% exposure were used in order to limit errors due to dead-time incurred by instrument mode switching. The light curve was binned to have greater than 20 counts/bin.

2.3. Fitting a composite BAT and XRT light curve

To investigate the connection between the prompt and the afterglow emission in the composite light curves, we first fit the XRT light curve, only using data where the hardness ratio showed no strong spectral evolution. We then fit both the BAT and XRT light curves jointly. Both fits were performed using a power-law model with an offset time (PLO),

$$F_{15-25\text{keV}} = K_{pow} (t - t_0^{pow})^{-\alpha}, \quad (2)$$

where t_0^{pow} is a offset time, α is a decay index, and K_{pow} is the normalization, and with an exponential model (EXP),

$$F_{15-25\text{keV}} = K_{exp} \exp\left(-\frac{t}{w}\right), \quad (3)$$

where w is the decay constant and K_{exp} is the normalization. For the XRT only fit, we fixed t_0^{pow} to zero. Finally, we fit the BAT and XRT light curves simultaneously using a combination of a power-law model with an exponential decay component (PLEXP),

$$F_{15-25\text{keV}} = K_{pow} (t - t_0^{pow})^{-\alpha} + K_{exp} \exp\left(-\frac{t}{w}\right). \quad (4)$$

For the fit to the XRT only light curve, the time interval was from the first XRT data point to the last data point before showing a deficit from the PLO model using an offset time of zero. For the joint BAT and XRT fit, the time interval was from the first BAT data point to the last XRT data point before showing a residual from the PLO model. Any other definitions used for the time interval are stated as a footnote in table 1. The values of the time intervals used in the light curve fitting are shown in the fourth column of table 1. The best-fit model was selected based on the χ^2 of the fit. However, because a PLO model will not fit the data before t_0^{pow} , the judgment between PLO and PLEXP is based on visual inspection as to whether the model fit both the BAT and XRT data simultaneously or not.

3. Results

The left panels of figures 2–6 show the composite BAT (black open circles) and XRT (red open triangles) light curve in the 15–25 keV band overlaid with the best-fit light curve model. The light curve models are PLO (eq. (2)), EXP (eq. (3)), and PLEXP (eq. (4)) from top to bottom. In the bottom figure of PLEXP, both PLO and EXP components are also shown as a dashed and a dash-dotted line, respectively. The best-fit parameters of the light curves are summarized in table 1. The best-fit of these models is labeled in blue. The right panels of figures 2–6 from top to bottom show the BAT light curve in the 15–150 keV band, the BAT photon index based on the time-resolved spectral analysis, the XRT 2–10 keV count rate, and the XRT count rate ratio (2.0–10.0) keV/(0.5–2.0) keV. The best-fit spectral parameters based on the 2–10 keV joint fit to the XRT WT and PC mode data are summarized in table 2.

From the initial steep decay phase of the XRT light curve, it is difficult to distinguish between PLO and EXP from the XRT data alone. Both models fit equally well for all of the bursts. However, the difference and the importance of the individual components become clear when the BAT data are included in the fit. An EXP model fits well for GRB 050814, GRB 050915B, GRB 060427 and GRB 060428B. A PLO or a PLEXP model is not required for these GRBs. For GRB 060923C, a PLO is the model best represented by the composite light curve. A PLEXP is the best model for the remaining 7 GRBs. The best-fit parameters which we used in the systematic study presented in this section, are shown in bold font in table 1.

First, we investigated the possibility of the curvature effect for those GRBs which have a PLO component in the composite BAT and XRT light curve fit. According to the curvature effect (Fenimore et al. 1996; Kumar & Panaitescu 2000; Zhang et al. 2006a), the relation between the decay index, α , and the XRT photon index, Γ_{XRT} , should be described by, α

$= 1 + \Gamma_{XRT}$, if the curvature effect is the cause of the XRT steep decay. Figure 7 shows the correlation between α and Γ_{XRT} for our sample. The dashed line is the expected relationship from the curvature effect ($\alpha = 1 + \Gamma_{XRT}$). Although GRB 060923C may be consistent with the curvature effect, the majority of the bursts in the sample do not satisfy the expected relation. The inconsistency with the curvature effect could be due to neglecting the spectral evolution during the steep decay in our analysis of the XRT data. Looking at the time evolution of the count rate ratio of our sample, we find a hard to soft evolution from 0.6 to 0.5 and from 0.6 to 0.4 for GRB 060202 and GRB 060211A. These changes correspond to an evolution of the photon index from 1.5 to 1.7 and from 1.5 to 1.9, respectively, according to the calculation by the Xspec *fakeit* command using the detector and the ancillary response files created for each source region. If this spectral evolution is taken into account, the steep decay could be consistent with the expectation of the curvature effect for GRB 060211A and GRB 060202. However, we do not see a strong spectral evolution for the other GRBs with the exception of GRB 060418. Note that for GRB 060418, there is a strong evolution in the hardness ratio during the episode at $t_0 + 150$ s which may cause an error in the extrapolated flux.

We find that most of the sample requires an EXP component to fit the BAT and XRT light curves simultaneously. Therefore, we can conclude that some of the early steep decay observed by XRT is a continuation of the exponential decay tail of the prompt emission. Interesting characteristics can be found for the bursts where a PLEXP model is the most representative model for the composite light curve. The dominant component of the fit to the XRT light curve 180 s after t_0 for GRB 060202 is an EXP. For GRB 050803 and GRB 060109 there is almost equal contribution from the EXP and PLO components in the initial XRT data. Whereas, a PLO is the dominant component for GRB 051109A, GRB 060111B, GRB 060211A, GRB 060306 and GRB 060418B. This result clearly demonstrates that the XRT steep decay could be composed of at least two different components. Without careful consideration of both the BAT and the XRT data simultaneously, it is not possible to distinguish between these two different components. It is important to note that O’Brien et al. (2006) also reached a similar conclusion; that the BAT and XRT composite light curve is composed of an exponential decay which relaxes to a power-law decay.

For the bursts that exhibit an EXP component, we investigated the correlation between the exponential decay index, w , and the prompt emission properties derived from the BAT data (table 3). The results are summarized in figure 8. No correlation is found for the properties of the prompt emission except between w and the BAT T_{90} which is expected because both parameters are related to the duration of the bursts.

Based on our study, there is a strong indication that the steep decay component observed

by the XRT is part of the prompt emission (e.g., also Nousek et al. 2006; O’Brien et al. 2006). Thus, we calculate the fluence which may be below the sensitivity limit of the BAT. This fluence was calculated by accumulating the flux from the best-fit composite BAT and XRT light curve model from the end of the emission as detected by the BAT to 1000 seconds after t_0 . Figure 9 shows the ratio of the percentage of the fluence in the tail emission which is below the BAT sensitivity limit and the fluence recorded by the BAT. For 7 out of the 13 GRBs in the sample, the fluence of the tail component is less than 15% of the fluence recorded by BAT. However, more than 15% of the fluence may be radiated below the BAT sensitivity limit for GRB 050915B, GRB 051109A, GRB 060202, GRB 060211A, GRB 060427, and GRB 060428B. This result gives rise to the question as to whether the fluence measured by the γ -ray instrument reflects the true fluence of the prompt emission.

4. Discussion

We have presented the BAT and XRT composite light curves, derived extrapolating the XRT 2–10 keV flux up to the BAT 15–25 keV energy range for GRBs which have a steep decay component in the initial XRT light curve. Based on the simultaneous fit of both the BAT and XRT light curves, we have confirmed the existence of an EXP component which smoothly connects the BAT prompt emission to the XRT steep decay for several GRBs. We have also found that the XRT steep decay for some of the bursts can be fit well by a PLEXP model. In the following sections, we discuss the possible origins of the PLO and EXP components.

4.1. Origin of the PLO component

A PLO component most likely originates from an internal shock (so called, curvature radiation or high-latitude emission associated with the last bright spike. Kumar & Panaitescu 2000; Nousek et al. 2006; Zhang et al. 2006a; Yamazaki et al. 2006). Our results support this idea, because for most bursts the XRT steep decay component smoothly connects with the last bright episode detected by the BAT (e.g. GRB 050803). The instantaneous emission from a uniform jet produces a decay index of $\alpha = 1 + \Gamma$ (Kumar & Panaitescu 2000). This formula was examined using the power-law decay index derived from the PLO model and the photon index based on the joint WT and PC spectral analysis of our sample. For the majority of the sample, we find that the decay index is not consistent with the formula. One of the possible reasons for this inconsistency could be the spectral evolution during the early XRT observation in some bursts (Zhang, Liang, & Zhang 2006). However, as discussed in

section 3, the inconsistency cannot always be associated with spectral evolution. Another possible reason is the choice of the time-zero (Zhang et al. 2006a; Yamazaki et al. 2006). Liang et al. (2006) investigated the curvature effect as an origin of the XRT steep decay using the data set of O’Brien et al. (2006). They made the assumption that the XRT steep decay component is due to the curvature effect and investigated whether the time-zero is consistent with the beginning of the bright episode. They concluded that for most of the sample, the time-zero was consistent with this picture. The main issue with their approach is that for the fixed power-law decay index, as expected from the formula $\alpha = 1 + \Gamma$, by shifting the offset time it is possible to fit the decay index to most early XRT data. This is because in their approach, the fitting parameters are not only the offset time but also the normalization, allowing extra freedom in the fit. Here, we demonstrate this problem using GRB 050803 and GRB 050814. The dash-dotted lines in figure 10 show the best fit PLO model by changing α from 1 to 5 for GRB 050803 and from 2 to 3 for GRB 050814, and varying t_0^{pow} . Only the XRT data, shown in red triangles, are used in the fitting process as in Liang et al. (2006). As seen in the figures, the choice of α and t_0^{pow} is not unique if one only try to fit the XRT data. Moreover, as it is clearly demonstrated in the case of GRB 050814, even if t_0^{pow} is chosen as the start time of the GRB pulse, the intensity of the pulse expected from the model is an order of magnitude brighter than the data. Therefore, if a bright episode in the BAT data, which could contribute to the steep decay component, is simultaneously fit with the XRT data, as in our approach, both the offset time and the decay index will be uniquely constrained by the data. It may be difficult to test the curvature effect or the relation $\alpha = 1 + \Gamma$ definitely without fitting the XRT and BAT data simultaneously. The third possibility is to abandon the assumption of the uniform jet emission. Our results may suggest that the structure of the jet is much more complex than a uniform jet (e.g. Yamazaki et al. 2006).

4.2. Origin of EXP component

Since it is difficult to explicitly state the origin of an EXP component, we will discuss the possibilities of both an internal shock and an external shock as the origin of an EXP component.

4.2.1. External shock scenario for EXP component

One interpretation of an EXP component is the presence of the external shock emission during the prompt phase. Fenimore & Ramirez-Ruiz (1999) studied the case of the

co-existence of the emission from the external shock (deceleration of the initial shell) during the emission from the internal shocks. They showed that the smooth long lasting soft emission which arose from an external shock could overlay the light curve of the prompt emission. Furthermore, Fenimore & Ramirez-Ruiz (1999) showed that the efficiency of converting the bulk energy to radiation is 85% in this case, whereas, internal shocks without deceleration only convert about 1% (Kumar 1999; Panaitescu et al. 1999). Zhang et al. (2006b) calculated the radiation efficiency using the *Swift* X-ray afterglow data and show that about half of the GRBs have an efficiency $\gtrsim 1\%$ which provides a challenge for producing the prompt emission from internal shocks alone. Furthermore, according to the optical observation by Rapid Telescopes for Optical Response (RAPTOR) during the prompt emission of GRB 050820A, smoothly decaying emission which does not correlate with the prompt spikes was found (Vestrand et al. 2006). If this emission is from the external shock, we might be observing the deceleration of the outflow during the prompt phase.

Following the argument of Fenimore et al. (1996) and Fenimore & Ramirez-Ruiz (1999), we estimate the bulk Lorentz factor of our sample, assuming an EXP component is purely due to external shock emission. Let us assume that an external shock starts its emission at the radius, R_0 . The external shock will be decelerated because of sweeping up the inter-stellar medium (ISM). The total energy of the central engine, E_0 , can be expressed as,

$$E_0 = (4\pi/3)R_0^3 n_{\text{ISM}} m_p c^2 \gamma_0^2 \quad (5)$$

where n_{ISM} is a density of the ISM, m_p is the proton mass, c is the speed of light, and γ_0 is the bulk Lorentz factor at R_0 . The duration of the emission (ΔT) is determined by the radial time scale (Piran 1999) which is the difference in the arrival time of the photons emitted between R_0 and aR_0 ($a > 1$) as measured by the observer,

$$\Delta T = [(a^4 - 1)/4](R_0/2\gamma_0^2 c).$$

Therefore, the bulk Lorentz factor can be expressed as,

$$\gamma_0 = (32\pi m_p c^2/3)^{-1/8} [(a^4 - 1)/4]^{3/8} (E_0/n_{\text{ISM}})^{1/8} (c\Delta T)^{-3/8}. \quad (6)$$

The relationship between ΔT and the full width at half maximum (FWHM) of the pulse ($T_{1/2}$) is described by, $0.22 \Delta T = T_{1/2}$, which is valid for a pulse shape of a fast rise, exponential decay (FRED) (Fenimore et al. 1996). Thus, once we know the redshift, since $T_{1/2}$ can be estimated from the best-fit parameters of an EXP component, we can calculate the bulk Lorentz factor as a function of E_0/n_{ISM} . In the following arguments, we use a typical value of 2 for the parameter “ a ” (in the $a = 2$ case, ΔT is the radial time scale from R_0 to $2R_0$).

For bursts with unknown redshifts (all bursts in the sample except GRB 050814, GRB 051109A and GRB 060418), we used the mean redshift of 2.4 obtained from the *Swift* long GRBs⁴. We can derive a reasonable range of γ_0 from 143 to 350 and R_0 of $\sim 10^{16}$ cm assuming $E_0/n_{\text{ISM}} = 1 \times 10^{52}$ erg cm³ for the 12 GRBs in our sample which have an EXP component in the best fit model (table 3). According to the calculation of γ_0 by the Rapid Eye Mount (REM) telescope using the peak time of the early afterglow data, γ_0 is about 400 for GRB 060418 and GRB 060607A (Molinari et al. 2006). Their γ_0 value agrees within a factor of two of our estimates. For GRB 060418, E_0 will be $\sim 1 \times 10^{54}$ ergs if we assume γ_0 of 400 as derived from the REM observation and n_{ISM} of 1 cm⁻³. E_0 of $\sim 10^{54}$ ergs is also a typical value according to the calculation of Zhang et al. (2006b) using X-ray afterglow data observed by XRT.

It would be interesting to look for a correlation between γ_0 and E_{peak} in the GRB rest frame ($E_{\text{peak}}^{\text{src}}$) although it is difficult to calculate for our sample because we do not have measurements of both E_{peak} and redshift. One of the advantages of using the *Swift* sample for this study is that soft GRBs, so called X-ray Flashes (XRFs), are included in the sample because of the relatively softer energy response of BAT compared to that of BATSE. In the dirty fireball model (Dermer et al. 1999), $E_{\text{peak}}^{\text{src}}$ has a strong dependency on the bulk Lorentz factor ($E_{\text{peak}}^{\text{src}} \propto \gamma_0^4$). The unified jet models for XRFs and GRBs, such as the structured-jet model (Rossi et al. 2002), and the variable jet opening angle model (Lamb et al. 2006; Donaghy 2006), expect a positive correlation between $E_{\text{peak}}^{\text{src}}$ and the bulk Lorentz factor. In the off-axis jet model (Yamazaki et al. 2004), no correlation is expected between γ_0 and $E_{\text{peak}}^{\text{src}}$ because the Doppler factor will change as a function of a viewing angle but not γ_0 . Another interesting theoretical model to discuss is the case of a very high Lorentz factor (Mochkovitch et al. 2003; Barraud et al. 2005). According to this model, XRFs can be produced in a condition with a very high γ_0 (so called “clean fireball”), while classical GRBs have a moderate γ_0 . In this case, we would expect a negative correlation between $E_{\text{peak}}^{\text{src}}$ and the bulk Lorentz factor. Some additional effort, for example, to estimate E_{peak} from the *Swift* BAT data (Sakamoto et al. in preparation) and to estimate a redshift from the *Swift* data (e.g., Grupe et al. 2006) is encouraged in order to discuss the correlation between γ_0 and $E_{\text{peak}}^{\text{src}}$ and the origin of XRFs.

We can derive another constraint on γ_0 which is independent of the previous discussion. Our observational results suggest that the photons originating from an internal shock via the curvature effect (PLO component) and photons from an external shock (EXP component) arrive at the observer almost simultaneously. The observed time of the photon from an

⁴http://heasarc.gsfc.nasa.gov/docs/swift/archive/grb_table/

internal shock, T_{int} , can be expressed as,

$$T_{int} \sim (R_{int}/2c\gamma_{int})[1 + (\gamma_{int}\theta)^2],$$

where R_{int} is the radius where an internal shock emits, γ_{int} is the bulk Lorentz factor at R_{int} , and θ is the jet opening half-angle. On the other hand, the observed time of an external shock emission, T_{ext} , is expressed as,

$$T_{ext} \sim R_{ext}/(4c\gamma_{ext}^2),$$

where R_{ext} is the radius where an external shock emits and γ_{ext} is a bulk Lorentz factor at R_{ext} (Sari 1998). If we assume $T_{int} \sim T_{ext}$ and also $\gamma_{int} \sim \gamma_{ext} \sim \gamma_0$, we have,

$$2R_{int}[1 + (\gamma_0\theta)^2] \sim R_{ext}.$$

$E_{\text{peak}}^{\text{src}}$ can be written as a function of θ and γ_0 ,

$$E_{\text{peak}}^{\text{src}}(\theta) \sim (2\gamma_0 h\nu'_0)[1 + (\gamma_0\theta)^2] \sim [E_{\text{peak}}^{\text{src}}(\theta = 0)]/(1 + (\gamma_0\theta)^2),$$

where $E_{\text{peak}}^{\text{src}}(\theta = 0)$ is E_{peak} observed by the on-axis observer. In this case, $E_{\text{peak}}^{\text{src}}(\theta = 0)$ corresponds to the observed E_{peak} multiplied by $(1+z)$. Therefore, the relationship between R_{int} , R_{ext} and E_{peak} is given by,

$$R_{ext}/2R_{int} \sim [E_{\text{peak}}(\theta = 0)]/E_{\text{peak}}(\theta).$$

Since the observed photon index of the XRT steep decay emission of our sample is ~ 2 , which suggests that the observation of the spectrum is above E_{peak} , it is reasonable to assume that the upper limit of $E_{\text{peak}}(\theta)$ is in the few keV range. Hence, the condition will be,

$$R_{ext}/2R_{int} > [E_{\text{peak}}(\theta = 0)]/E_{\text{peak}}(\theta')$$

where $E_{\text{peak}}(\theta')$ is the upper limit of a few keV. If we use the angular spreading time (ΔT_{ang}) (Piran 1999) as the time scale of an internal shock, then,

$$R_{int} \sim 2c\gamma_0\Delta T_{ang}.$$

From Eq. (5), the radius of an external shock can be expressed as

$$R_{ext} = (4\pi m_p c^2/3)^{-1/3}(E_0/n_{ISM})^{1/3}\gamma_0^{-2/3}.$$

Thus, γ_0 can be written as,

$$\gamma_0 > (1/4)^{3/8}(4\pi m_p c^2/3)^{-1/8}(E_0/n_{ISM})^{1/8}(c\Delta T_{ang})^{-3/8}[E_{\text{peak}}(\theta = 0)/E_{\text{peak}}(\theta')]^{-3/8}. \quad (7)$$

In the case of GRB 050803, ΔT_{ang} can be derived as the duration of the last spike (the pulse at t_0+90 s), $\Delta T_{ang} \sim 3$ s, if one takes into account the time dilation effect. Although it is not possible to extract the information about the E_{peak} of this pulse from the BAT data, it is reasonable to assume $E_{peak} > 100$ keV since the photon index from a simple power-law fit to the BAT data is 1.2 ± 0.2 which is close to the low energy photon index of the typical GRB spectrum (E_{peak} should be around or above the BAT upper energy range of 150 keV). Therefore, we use $E_{peak}(\theta = 0)/E_{peak}(\theta') > 100$. The lower limit of γ_0 of GRB 050803 is estimated to be < 50 assuming a redshift of 2.4 (the mean redshift of the *Swift* long GRBs) and E_0/n_{ISM} of 1×10^{52} ergs cm³. Applying the same assumptions for the GRB spectral parameters ($E_{peak}(\theta = 0)/E_{peak}(\theta') > 100$), we estimate a lower limit of < 60 for GRB 060418 using the measured redshift of 1.489, ΔT_{ang} of 2 s (the pulse at t_0+50 s), and E_0/n_{ISM} of 1×10^{52} ergs cm³. The estimated lower limit of γ_0 for GRB 060418 is not contradicted by the value based on the REM observation. In summary, for the EXP component, one can provide a reasonable bulk Lorentz factor, γ_0 , within the external shock scenario, which is consistent with other measurements.

4.2.2. Internal shock scenario for EXP component

As we discussed in §4.1, a simple interpretation based on a uniform jet model could contradict the prediction of the curvature effect. Here we discuss an internal shock scenario for both EXP and PLO components based on an inhomogeneous jet model. Yamazaki et al. (2006) investigated the GRB prompt emission 100-1000 seconds after the GRB trigger within the frame work of a multiple sub-shell model. According to their study, despite an angular inhomogeneity of the jet, the tail emission has a monotonic decay which resembles the XRT steep decay. In this context, if the jet has a core in which the emission energy is densely confined compared with the outer region, the PLO decay component arising from an on-beam sub-shell may be overlaid by the off-beam core emission which causes the EXP decaying component. Takami et al. (2007) further extended their study, and in order to investigate the unknown jet structure, they proposed unique definitions of the decay index derived by unique definitions of the time-zero and of the fitting interval of the observed light curve. They found that the decay index in their definitions should have a wide scatter in the case of a power-law like structured jet. Here, we calculated the decay index using our BAT and XRT composite light curve based on the definitions of Takami et al. (2007). Because of the difficulty of using exactly the same definition of time-zero as proposed in Takami et al. (2007) (T_* in their paper), we define the end of the BAT emission as T_* . We can fit our light curves using the proposed fitting interval for five GRBs in our sample (α_{tail} as a decay index, χ^2 and d.o.f. of the fits are shown in the last two columns of table 3).

Our results, based on a very small sample, show that the decay index ranges from 0.6 to 3.0. However, both the size of the sample and the number of data points included in the light curve fit are very small because of using XRT data above 2 keV. There is an additional issue further reducing the sample; the appearance of a shallow decay in the XRT data in the fitting interval. Unfortunately, it is hard to conclude the structure of a jet with our limited sample. Once the GRB sample suitable for fitting a light curve with the unique definitions of Takami et al. (2007) can be increased, we may be able to draw a conclusion about the jet structure of GRBs using the XRT steep decay component.

5. Summary

In this paper, we presented a systematic study of the steep decay emission observed by the XRT. We constructed composite light curves in the 15–25 keV band extrapolating the XRT data (2–10 keV) up to the BAT energy range (15–25 keV). Based on the simultaneous fitting of the BAT and XRT data, we confirmed the existence of an EXP component for the majority of the bursts in the sample. We found that for the PLO component, the majority of the GRBs in our sample are inconsistent with the relationship of the curvature effect, $\alpha = \Gamma + 1$, which is only valid in the case of the uniform jet. We also found that more than 15% of the prompt fluence may be radiated below the BAT sensitivity limit for half of our sample. We argue that the EXP component could be the emission from the external shock which may indicate the deceleration of the initial shell by ISM during the prompt phase. We discuss the case of the prompt tail emission from the structured jet as an origin of the XRT steep decay but the sample is too small for a solid conclusion.

We would like to thank A. P. Beardmore, G. Chincarini, C. Guidorzi, P. T. O’Brien and K. L. Page for valuable comments. We also would like to thank the anonymous referee for comments and suggestions that materially improved the paper. This research was performed while T. S. held a NASA Postdoctoral Program administered by Oak Ridge Associated Universities at NASA Goddard Space Flight Center. R. Y. was supported in part by Grants-in-Aid for Scientific Research of the Japanese Ministry of Education, Culture, Sports, Science, and Technology 18740153. The material of the paper has been improved by the discussions during the workshop “Implications of *Swift*’s Discoveries about Gamma-Ray Bursts” at the Aspen Center for Physics.

REFERENCES

- Band, D.L., et al. 1993, ApJ, 413, 281
- Barraud, C. et al. 2005, A&A, 440, 809
- Barthelmy, S.D. et al. 2005, Space Sci. Rev., 120, 143
- Barthelmy, S.D. et al. 2006, ApJ, 635, L133
- Burrows, S.D. et al. 2005, Space Sci. Rev., 120, 165
- Butler, N.R., Kocevski, D. 2007, Submitted to ApJ (astro-ph/0702638)
- Dermer, C.D., Chiang, J., & Mättcher, M. 1999, ApJ, 656
- Donaghy, T. Q. 2006, ApJ, 645, 436
- Dupree, A.K. et al. 2006, GCN Circ. 4969, <http://gcn.gsfc.nasa.gov/gcn3/4969.gcn3>
- Fenimore, E.E., Madras, C.D., & S. Nayakshin 1996, ApJ, 473, 998
- Fenimore, E.E. & Ramirez-Ruiz, E. 1999, Submitted to ApJ (astro-ph/9909299)
- Frontera, F. et al. 1999, ApJS, 127, 59
- Gehrels, N. et al. 2004, ApJ, 611, 1005
- Giblin, T.W. et al. 1999, ApJ, 524, L47
- Giblin, T.W. et al. 2002, ApJ, 570, 537
- Grupe, D. et al. 2007, AJ, 133, 2216
- Hill, J.E., et al. 2004, Proc. SPIE, 5165, 217
- Hill, J.E., et al. 2005, Proc. SPIE, 5898, 313
- Jakobsson, P. et al. 2006, in AIP Conf. Proc. 836, Gamma-ray bursts in the *Swift* era, ed. S.S.Holt, N. Gehrels, and J.A.Nousek (New York: AIP), 552
- Kaneko, Y. et al. 2006, ApJS, 166, 298
- Kennea, J.A. et al. 2005, Proc. SPIE, 5898, 341
- Kumar, P. 1999, ApJ, 523, L113

- Kumar, P. & Panaitescu, A. 2000, ApJ, 541, L51
- Lamb, D.Q., Donaghy, T.Q., & Graziani, C. 2006, ApJ, 520, 335
- Lloyd-Ronning, N.M., Petrosian, V. 2002, ApJ, 565, 182
- Liang, E.W. et al. 2006, ApJ, 646, 351
- Markwardt, C.B. et al. 2005, ApJ, 633, L77
- Mészáros, P., & Rees, M. 1997, ApJ, 476, 232
- Mochkovitch, R., Daigne, F., Barraud, C., & Atteia, J. L. 2003, in APS Conf. Ser. 312, Third Rome Workshop on Gamma-Ray Bursts in the Afterglow Era, ed. M. Feroci et al. (San Francisco: ASP), 381
- Molinari, E. et al. 2007, A&A in press (astro-ph/0612607)
- Moretti, A. et al. 2004, Proc. SPIE, 5165, 232
- Nousek, J.A. et al. 2006, ApJ, 642, 389
- O’Brien et al. 2006, ApJ, 647, 1213
- Panaitescu, A., Spada, M., & Mészáros, P. 1999, ApJ, 522, L105
- Panaitescu, A., & Kumar, P. 2002, ApJ, 571, 779
- Pian, E. et al. 2001, A&A, 372, 456
- Piran, T. 1999, Physics Reports, 314, 575
- Piro, L. et al. 2005, ApJ, 623, 314
- Quimby, R. et al. 2005, GCN Circ. 4221, <http://gcn.gsfc.nasa.gov/gcn3/4221.gcn3>
- Rees, M., & Mészáros, P. 1994, ApJ, 430, L93
- Romano, P., et al. 2006, A&A, 456, 917
- Rossi, E., Lazzati, D., & Rees, M.J. 2002, MNRAS, 332, 945
- Ryde, F. & Svensson, R. 2002, ApJ, 566, 210
- Sakamoto et al. 2005, ApJ, 629, 311
- Sari, R., & Piran, T. 1997, ApJ, 485, 270

- Sari, R. 1998, ApJ, 494, L49
- Sari, R., Piran, T., & Narayan, R. 1998, ApJ, 497, L17
- Scargle, J. D. 1998, ApJ, 504, 405
- Tagliaferri, G. et al. 2005, Nature, 436, 985
- Takami, K., Yamazaki, R., Sakamoto, T. & Sato, G 2007, ApJ in press (arXiv:0704.1055)
- Vaughan, S., et al. 2006, ApJ, 638, 920
- Vestrand, W.T. et al. 2006, Nature, 442, 172
- Willingale, R. et al. 2007, ApJ in press (astro-ph/0612031)
- Yamazaki, R., Ioka, K., & Nakamura, T. 2004, ApJ, 607, L103
- Yamazaki, R., Toma, K., Ioka, K., & Nakamura, T. 2006, MNRAS, 369, 311
- Yost, S. A., Harrison, F. A., Sari, R., & Frail, D. A. 2003, ApJ, 597, 459
- Zhang, B. et al. 2006a, ApJ, 642, 354
- Zhang, B. et al. 2006b, ApJ, 655, 989
- Zhang, B.B., Liang, E., Zhang, B. 2006, ApJ in press (astro-ph/0612246)

Table 1. Parameters of the light curve fits. Errors quoted at 68% confidence level. See text for details (section 2.3 and 3).

GRB	t_0 UT	Data [†]	Fitting [s]	Power-law				Exponential		
				t_0^{pow}	α	K_{pow}	χ^2/dof	w	K_{exp}	χ^2/dof
050803	2005-08-03 19:14:59.3	XRT	100–147	0^\dagger	5.3 ± 0.7	17.4	6.6 / 5	22 ± 3	$3.8^{+4.0}_{-1.9} \times 10^{-8}$	7.3 / 5
		PL/EX	0–406	$87.2^{+0.3}_{-0.4}$	1.18 ± 0.07	$(1.1 \pm 0.3) \times 10^{-8}$	14.4 / 10	32.3 ± 0.9	$(8.4 \pm 0.7) \times 10^{-9}$	122.2 / 13
		PLE	0–406	$88.3^{+0.03}_{-0.05}$	0.87 ± 0.03	$2.0 \times 10^{-9\dagger}$	–	26 ± 1	$1.0 \times 10^{-8\dagger}$	22.0 / 12
050814	2005-08-14 11:38:55.4	XRT	167–466	0^\dagger	3.6 ± 0.3	$4.1^{+6.2}_{-2.4} \times 10^{-2}$	11.7 / 20	71 ± 4	4.0×10^{-9}	23.7 / 20
		PL/EX	0–466	70.3	2.5	5.3×10^{-5}	10.3 / 21	66 ± 2	$(5.0 \pm 0.5) \times 10^{-9}$	27.7 / 23
		PLE	0–466	44.5	1.6	$5.1 \times 10^{-8\dagger}$	–	62 ± 1	$5.8 \times 10^{-9\dagger}$	24.2 / 22
050915B	2005-09-15 21:22:56.6	XRT	158–228	0^\dagger	5.3 ± 0.8	1.3×10^2	10.7 / 5	36^{+6}_{-5}	$2.1^{+2.7}_{-1.2} \times 10^{-8}$	11.7 / 5
		PL/EX	7–228	21.3	2.1	4.0×10^{-6}	27.0 / 7	33.2 ± 0.6	$(3.0 \pm 0.1) \times 10^{-8}$	27.6 / 8
		PLE	7–228	-29^{+11}_{-10}	$3.8^{+0.3}_{-0.2}$	$2.0 \times 10^{-2\dagger}$	–	35^{+2}_{-4}	$1.7 \times 10^{-8\dagger}$	16.4 / 7
051109A	2005-11-09 01:12:17.6	XRT	131–196	0^\dagger	2.2 ± 0.7	3.2×10^{-6}	0.4 / 4	74^{+36}_{-19}	$5.0^{+5.2}_{-2.5} \times 10^{-10}$	0.3 / 10
		PL/EX	0–196	1.9	–1.6	2.2×10^{-7}	7.8 / 6	28 ± 1	$(1.5 \pm 0.2) \times 10^{-8}$	50.8 / 8
		PLE	0–196	4.78 ± 0.02	0.79 ± 0.03	$2.5 \times 10^{-9\dagger}$	–	21 ± 3	$1.5 \times 10^{-8\dagger}$	2.8 / 7
060109	2006-01-09 16:54:41.2	XRT	110–200	0^\dagger	4.3 ± 0.4	2.6×10^{-1}	7.3 / 8	33 ± 3	$8.6^{+4.0}_{-2.7} \times 10^{-9}$	8.5 / 8
		PL/EX	0–862	88 ± 1	1.6 ± 0.1	$7.1^{+3.7}_{-2.2} \times 10^{-8}$	11.1 / 11	42 ± 2	$(3.6 \pm 0.4) \times 10^{-9}$	109.1 / 12
		PLE	0–862	90 ± 0.3	1.42 ± 0.03	$1.8 \times 10^{-8\dagger}$	–	32 ± 2	$3.5 \times 10^{-9\dagger}$	8.4 / 11
060111B	2006-01-11 20:15:41.2	XRT	89–149	0^\dagger	2.8 ± 0.7	2.1×10^{-5}	2.6 / 3	43^{+14}_{-9}	$6.5^{+6.2}_{-3.3} \times 10^{-10}$	3.2 / 3
		PL/EX	0–149	50	2.4	9.3×10^{-7}	13.0 / 6	23 ± 1	$(5.7 \pm 0.7) \times 10^{-9}$	133.3 / 7
		PLE	0–149	50.1 ± 0.3	2.38 ± 0.03	$7.5 \times 10^{-7\dagger}$	–	13 ± 2	$7.2 \times 10^{-9\dagger}$	14.5 / 6
060202	2006-02-02 08:40:29.9	XRT	250–350	0^\dagger	2.2 ± 0.3	8.7×10^{-5}	14.8 / 18	138^{+20}_{-16}	$3.5^{+1.1}_{-0.8} \times 10^{-9}$	15.2 / 18
		PL/EX	0–350 ^a	135^{+6}_{-8}	1.2 ± 0.2	1.8×10^{-7}	20.0 / 24	141 ± 6	$(3.4 \pm 0.3) \times 10^{-9}$	118.2 / 27
		PLE	0–350	127 ± 5	2.4 ± 0.1	$1.3 \times 10^{-5\dagger}$	–	141 ± 5	$2.8 \times 10^{-9\dagger}$	22.1 / 26
060211A	2006-02-11 09:39:59.9	XRT	232–312	0^\dagger	2.1 ± 0.9	1.6×10^{-5}	5.0 / 6	127^{+96}_{-39}	$8.3^{+12.2}_{-5.0} \times 10^{-10}$	5.2 / 6
		PL/EX	0–913	72	2.3	1.7×10^{-5}	43.8 / 29	81 ± 2	$(3.6 \pm 0.2) \times 10^{-9}$	333.0 / 32
		PLE	0–913	72	2.29 ± 0.02	$1.4 \times 10^{-5\dagger}$	–	54 ± 4	$3.1 \times 10^{-9\dagger}$	39.9 / 31
060306	2006-03-06 00:49:09.3	XRT	97–147	0^\dagger	3.7 ± 0.8	2.2×10^{-3}	3.1 / 2	31^{+9}_{-6}	$1.7^{+2.2}_{-1.0} \times 10^{-9}$	3.3 / 2
		PL/EX	35–256	40	2.3	1.1×10^{-6}	31.4 / 4	17.8 ± 0.7	$(3.1 \pm 0.7) \times 10^{-8}$	145.6 / 6
		PLE	35–256	40	2.33 ± 0.02	$1.0 \times 10^{-6\dagger}$	–	13 ± 1	$2.5 \times 10^{-8\dagger}$	25.4 / 5
060418	2006-04-18 03:05:49.2 ^b	XRT	178–400	0^\dagger	2.6 ± 0.1	$3.1^{+3.8}_{-1.7} \times 10^{-4}$	27.1 / 28	101 ± 6	$(2.0 \pm 0.3) \times 10^{-9}$	31.6 / 28
		PL/EX	108–797 ^c	146 ± 2	1.07 ± 0.08	$2.2^{+1.2}_{-0.8} \times 10^{-8}$	25.0 / 30	262 ± 23	$(3.0 \pm 0.5) \times 10^{-10}$	123.0 / 31
		PLE	108–797 ^b	148.7 ± 0.3	0.89 ± 0.01	$7.5 \times 10^{-9\dagger}$	–	43 ± 3	$1.5 \times 10^{-8\dagger}$	23.4 / 30
060427	2006-04-27 11:43:01.0	XRT	148–198	0^\dagger	4.4 ± 1.3	4.8×10^{-1}	3.7 / 3	41^{+20}_{-10}	$5.1^{+14.8}_{-0.3} \times 10^{-9}$	4.0 / 3
		PL/EX	0–218	66	2.8	3.7×10^{-5}	3.5 / 3	47 ± 2	$(2.9 \pm 0.4) \times 10^{-9}$	5.1 / 6
		PLE	0–218	114	6.9	2.7^\dagger	–	47	$2.8 \times 10^{-9\dagger}$	3.3 / 5
060428B	2006-04-28	XRT	235–340	0^\dagger	5.0 ± 0.7	74	7.9 / 7	55^{+10}_{-7}	$4.1^{+4.6}_{-2.1} \times 10^{-9}$	9.4 / 7

Table 1—Continued

GRB	t_0 UT	Data [‡]	Fitting [s]	Power-law				Exponential		
				t_0^{pow}	α	K_{pow}	χ^2/dof	w	K_{exp}	χ^2/dof
060923C	08:54:15.2	PL/EX	0–340	229	0.7	3.5×10^{-10}	2.9 / 6	48 ± 0.9	8.9×10^{-9}	$10.4 / 8$
		PLE	0–340	236^{+1}_{-2}	0.40 ± 0.05	$6.8 \times 10^{-11\dagger}$	2.7 / 7	39 ± 2	$1.0 \times 10^{-8\dagger}$	2.7 / 7
	2006-09-23 13:33:10.8	XRT	205–529	0 [†]	2.7 ± 0.3	1.7×10^{-4}	3.5 / 5	115^{+17}_{-14}	4.0×10^{-10}	5.4 / 5
		PL/EX	0–529	-3 ± 2	2.76 ± 0.02	$2.0 \times 10^{-4\dagger}$	$3.5 / 6$	43 ± 1	$(1.3 \pm 0.2) \times 10^{-8}$	45.3 / 6
		PLE	0–529	-2.9 ± 6	2.42 ± 0.03	$2.6 \times 10^{-5\dagger}$	3.2 / 5	33^{+4}_{-10}	$9.5 \times 10^{-9\dagger}$	3.2 / 5

[‡]XRT: fitting only the XRT data with a PLO model and an EXP model, PL/EX: joint BAT and XRT fit with a PLO model and an EXP model, PLE: joint BAT and XRT fit with a PLEXP model.

[†]Fixed value.

^aAll the BAT data points and the XRT data from t_0+224 s to t_0+350 s are used in the fit.

^bAlthough *battblocks* found a time interval which is 63 second before t_0 , we concluded that this interval is due to the contamination of Sco X-1 in the BAT field of view based on the BAT image analysis.

^cThe fit to the XRT data is from t_0+108 s to t_0+148 s, and from t_0+797 s to t_0+400 s. The BAT data points from t_0+146 s to t_0+156 s are also included in the fit.

Table 2. XRT spectral parameters based on a joint fit to WT and PC data using data above 2 keV. The error in the photon index is quoted at the 90% confidence level.

GRB	WT Fitting Range [s]	PC Fitting Range [s]	Γ_{XRT}	χ^2/dof
050803	100.1–184.1	185.5–12976	1.9 ± 0.2	33.0 / 37
050814	166.6–384.9	386.5–14133	2.1 ± 0.2	33.5 / 35
050915B	158.4–313.3	229.9–13791	1.8 ± 0.3	9.3 / 11
051109A	131.4–214.3	3444–17540	2.2 ± 0.2	19.0 / 31
060109	109.8–200.2	201.6–12559	2.0 ± 0.2	23.7 / 21
060111B	89.2–426.7	155.4–12655	2.2 ± 0.3	10.0 / 14
060202	175.1–1025	1028–13027	$1.99^{+0.05}_{-0.04}$	364.6 / 337
060211A	137.1–330.9	332.5–13054	1.8 ± 0.1	68.6 / 66
060306	96.9–174.5	175.8–12874	2.40 ± 0.03	9.8 / 15
060418	166.1–697.7	699.9–12561	$2.00^{+0.07}_{-0.06}$	211.7 / 209
060427	148.2–236.5	237.9–12691.	2.0 ± 0.4	7.7 / 10
060428B	235.6–440.8	442.7–12773	2.6 ± 0.3	16.6 / 17
060923C	204.6–267.4	268.7–12796	2.1 ± 0.4	3.0 / 7

Table 3. BAT prompt emission properties, and the estimated Bulk Lorentz factor, γ_0 , and the radius of the external shock, R_0 based on the external shock model. The XRT decay index based on the definition of Takami et al. (2007), α_{tail} , and χ^2 of the fit are also shown. Errors quoted the 68% confidence level.

GRB	T ₉₀ [s]	Model [★]	Γ_{BAT}	E_{peak} [keV]	S_E^a	F_E^{peakb}	S3/S2 ^c	z	T _{1/2}	γ_0^\dagger	R_0 [cm]	α_{tail}	$\chi^2/\text{d.o.f.}$
050803	87.9	PL	1.39 ± 0.07	—	22 ± 1	8.1 ± 0.7	1.5 ± 0.1	—	18	270	2.8×10^{16}	—	—
050814	140.6	PL	1.8 ± 0.1	—	19 ± 1	6.2 ± 1.2	1.2 ± 0.1	5.3 ¹	45	240	3.0×10^{16}	—	—
050915B	40.9	CPL	1.4 ± 0.2	60_{-5}^{+7}	34 ± 1	17 ± 1	1.05 ± 0.04	—	24	242	3.0×10^{16}	—	—
051109A	37.2	PL	1.5 ± 0.1	—	22 ± 2	29 ± 3	1.4 ± 0.2	2.346 ²	15	287	2.7×10^{16}	0.59 ± 0.05	9.7 / 14
060109	115.4	PL	1.9 ± 0.1	—	6.6 ± 0.6	3.4 ± 0.1	1.0 ± 0.2	—	23	246	3.0×10^{16}	—	—
060111B	58.8	PL	1.0 ± 0.1	—	16 ± 1	14 ± 2	2.0 ± 0.1	—	9	350	2.4×10^{16}	0.9 ± 0.1	1.0 / 3
060202	198.9	PL	1.8 ± 0.1	—	22 ± 1	3.7 ± 0.8	1.2 ± 0.1	—	98	143	4.3×10^{16}	—	—
060211A	126.3	CPL	0.9 ± 0.3	58_{-5}^{+8}	16 ± 1	3.3 ± 0.1	1.1 ± 0.1	—	24	242	3.0×10^{16}	1.3 ± 0.2	1.0 / 2
060306	61.2	PL	1.80 ± 0.05	—	21 ± 1	47 ± 2	1.1 ± 0.1	—	46	190	3.5×10^{16}	1.2 ± 0.2	2.4 / 3
060418	103.1	PL	1.64 ± 0.03	—	80 ± 1	49 ± 2	1.28 ± 0.03	1.489 ³	21	226	3.1×10^{16}	—	—
060427	64	PL	1.9 ± 0.2	—	5.0 ± 0.5	1.7 ± 0.7	1.1 ± 0.2	—	32	217	3.2×10^{16}	—	—
060428B	57.9	PL	2.6 ± 0.1	—	8.2 ± 0.5	3.4 ± 0.6	0.7 ± 0.1	—	27	232	3.1×10^{16}	3.0 ± 0.3	4.7 / 8
060923C	75.8	PL	2.3 ± 0.1	—	16 ± 1	5.0 ± 1.5	0.8 ± 0.1	—	—	—	—	—	—

[★]PL: power-law ($dN/dE \sim E^{-\Gamma_{BAT}}$), CPL: cutoff power-law ($dN/dE \sim E^{-\Gamma_{BAT}} \exp(-(2 - \Gamma_{BAT})E/E_{peak})$)

[†]Calculated bulk Lorentz factor assuming $E_0/n = 1 \times 10^{52}$ erg cm³.

^aEnergy fluence in the 15–150 keV band [10^{-7} erg cm⁻²]

^b1-s peak energy flux in the 15–150 keV band [10^{-8} erg cm⁻² s⁻¹]

^cFluence ratio between S3(50–150 keV)/S2(25–50 keV)

¹Jakobsson et al. (2006)

²Quimby et al. (2005)

³Dupree et al. (2006)

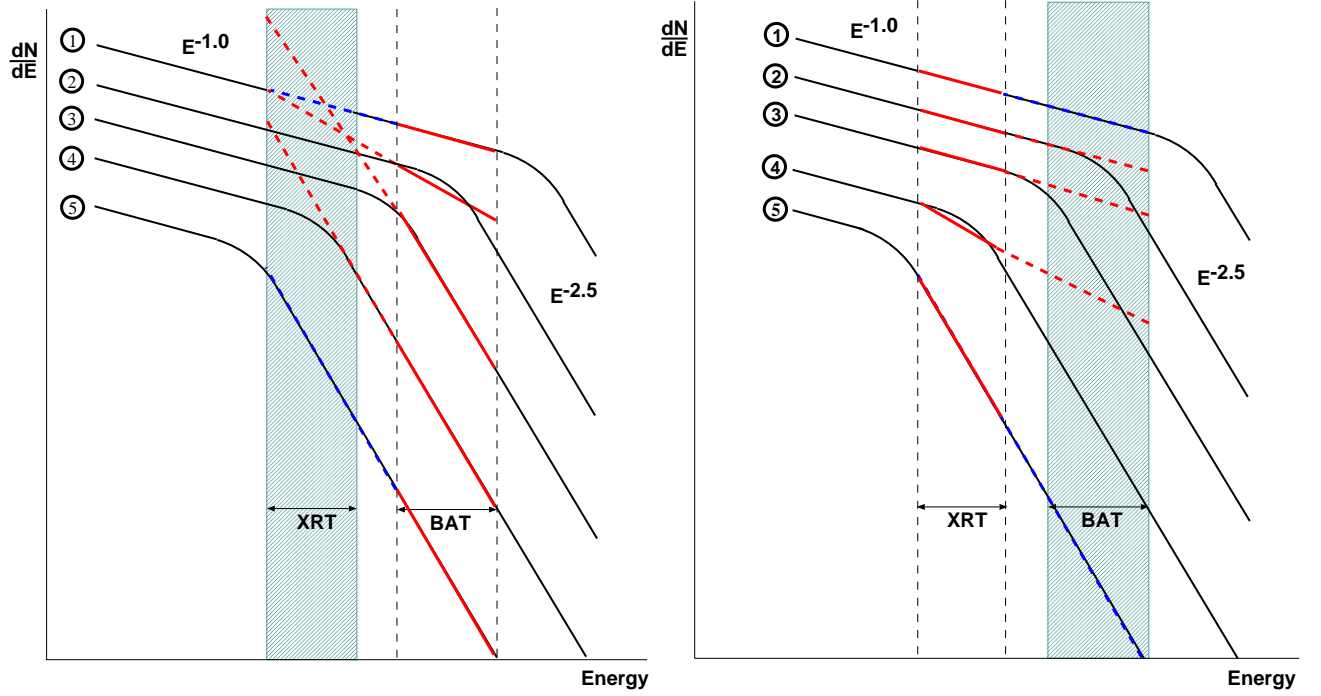


Fig. 1.— Schematic figures of the observed spectra with different E_{peak} energies (case 1: $E_{\text{peak}} > 150$ keV, case 2: $15 \text{ keV} < E_{\text{peak}} < 150$ keV, case 3: $10 \text{ keV} < E_{\text{peak}} < 15$ keV, case 4: $0.3 \text{ keV} < E_{\text{peak}} < 10$ keV, and case 5: $E_{\text{peak}} < 0.3$ keV) demonstrating issues with the different extrapolations (left: extrapolating the BAT data down to the XRT energy band (BAT-to-XRT extrapolation); right: extrapolating the XRT data up to the BAT energy range (XRT-to-BAT extrapolation)). The light blue hatched regions show the extrapolated energy band. The extrapolated spectra shown with red dotted lines indicate issue with the extrapolation. There should be no issue with the extrapolation of the spectra shown in case 1 and 5 (blue dotted lines). See text for details (section 1).

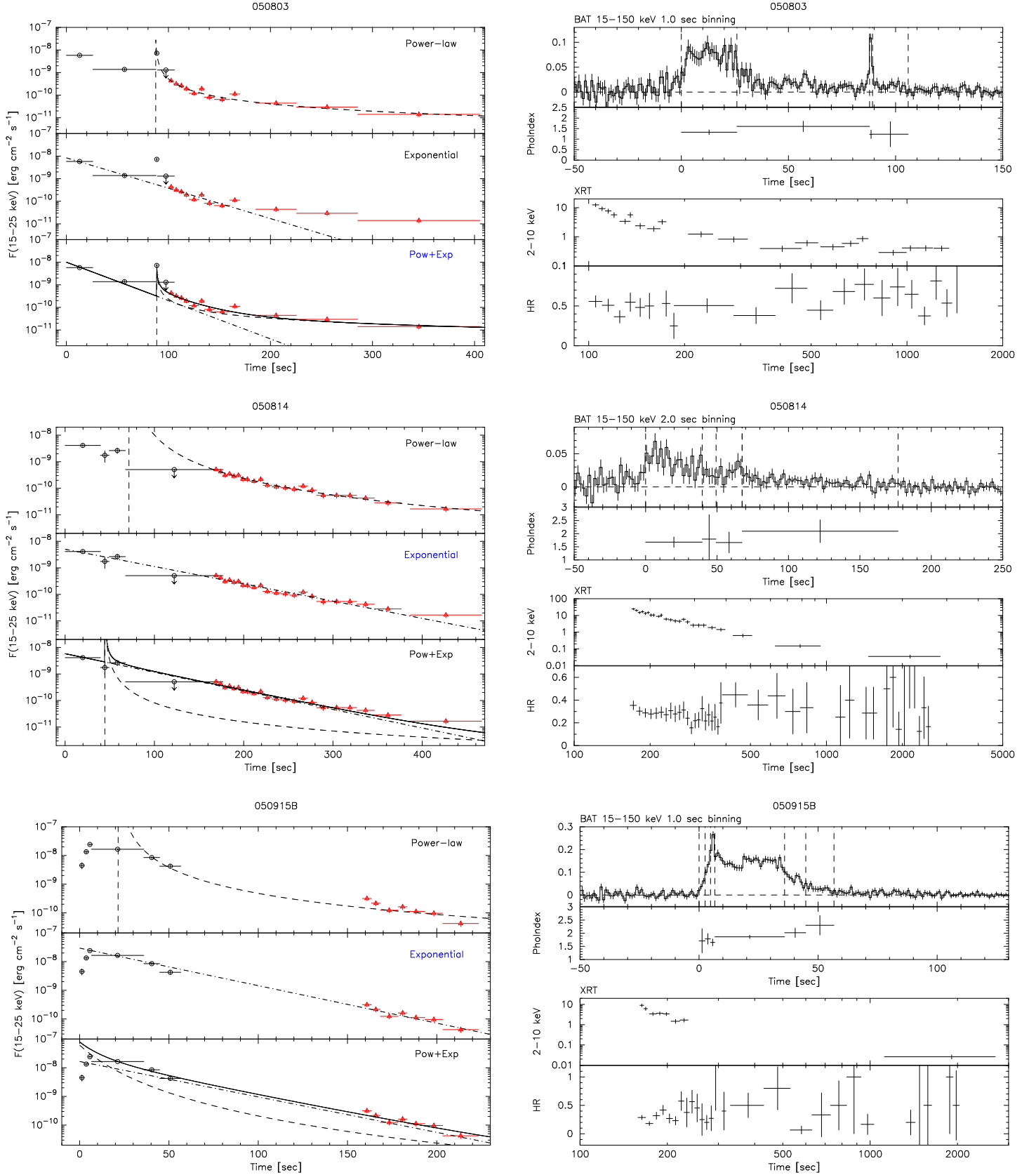


Fig. 2.— The BAT and XRT composite light curve. See text for details (section 3).

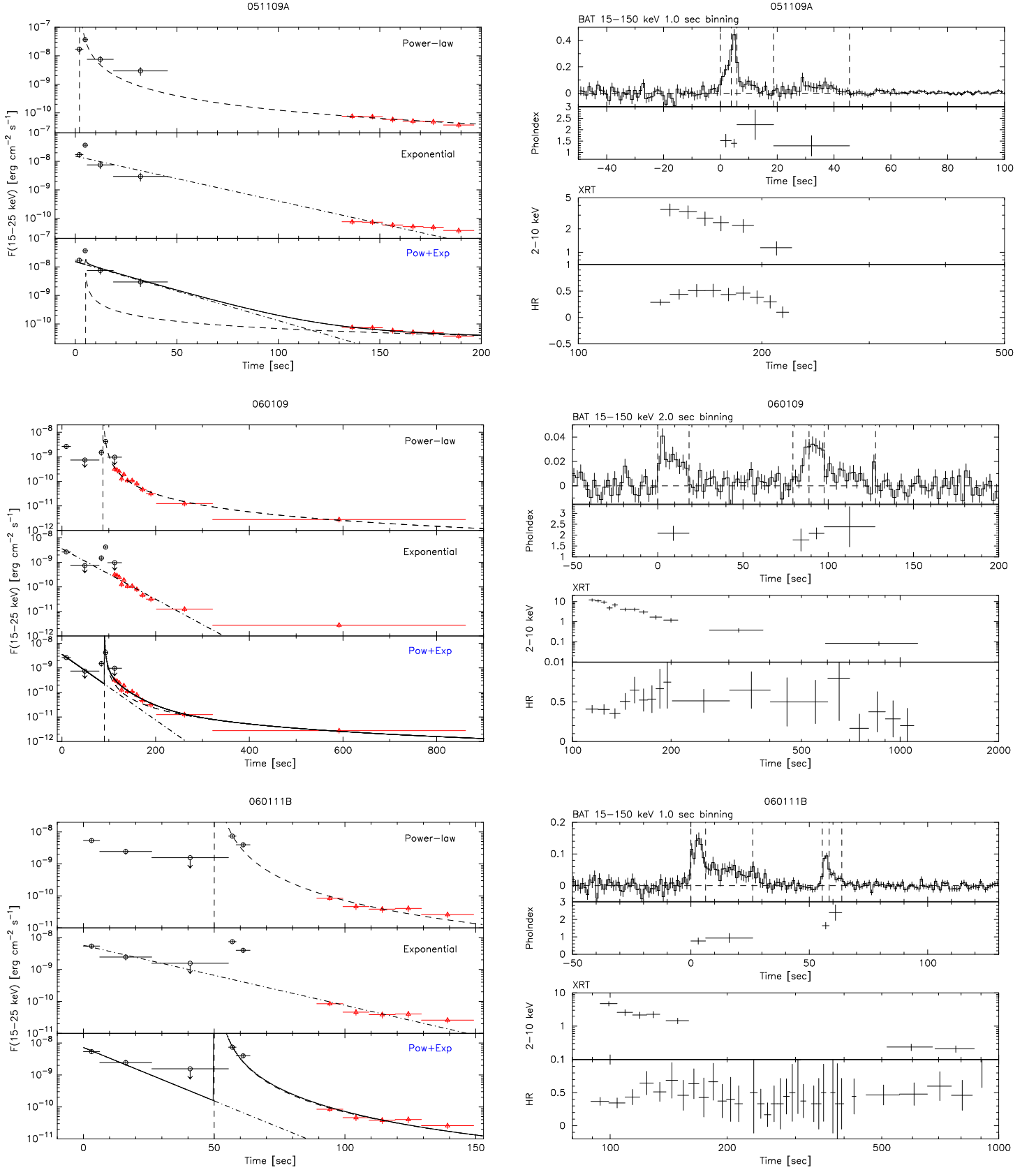


Fig. 3.— continued.

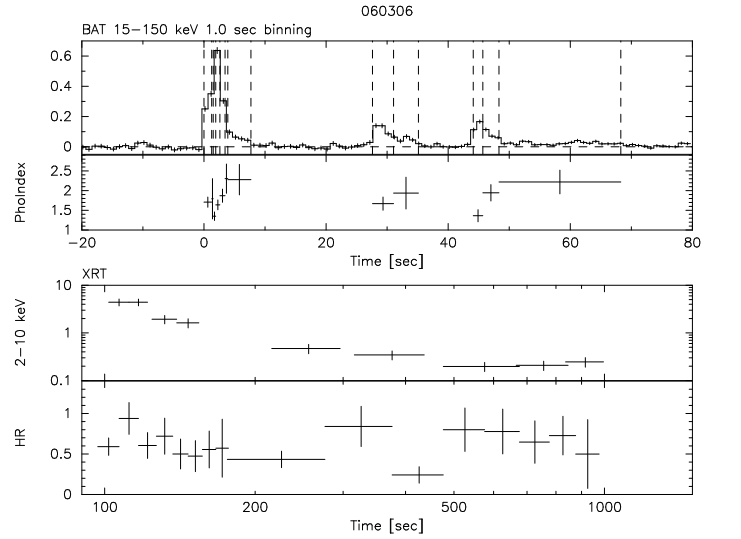
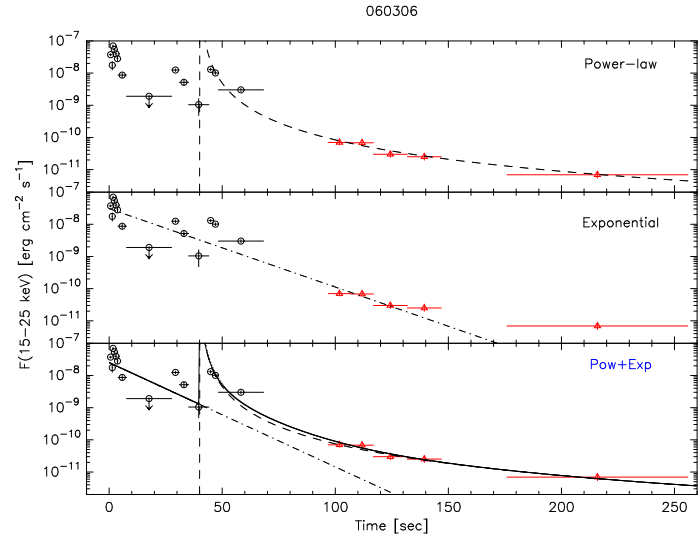
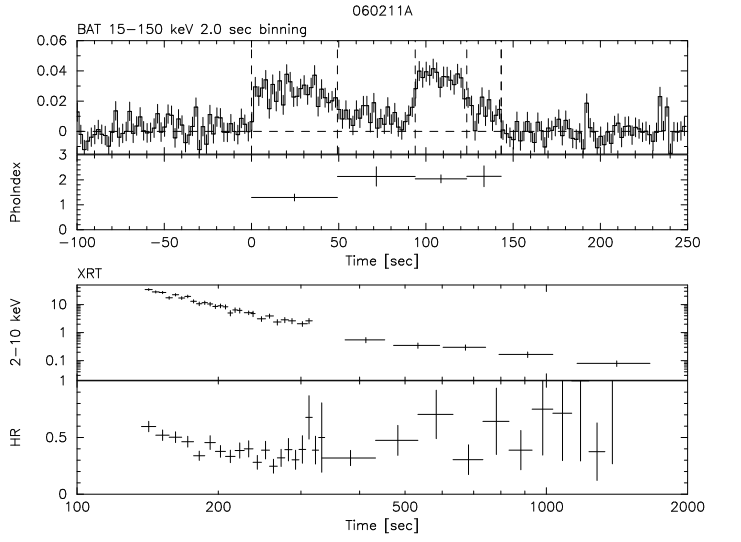
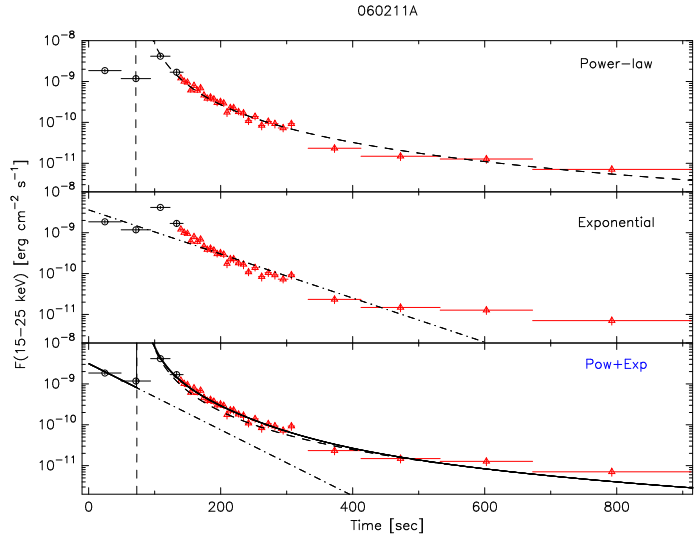
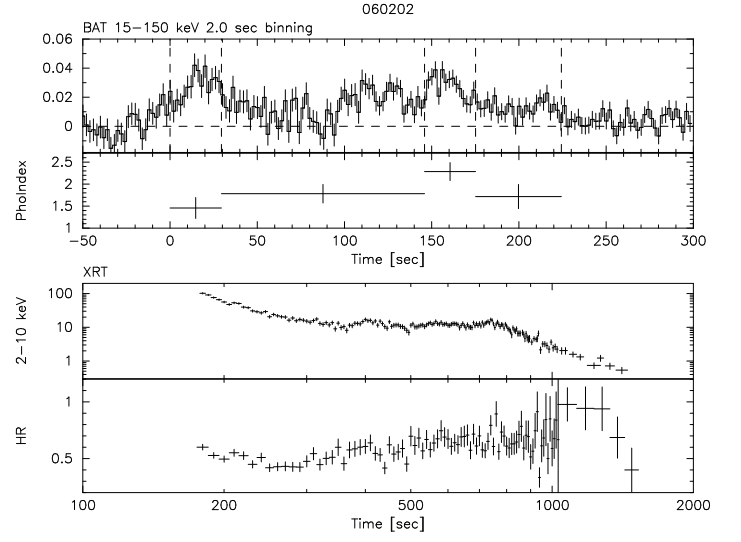
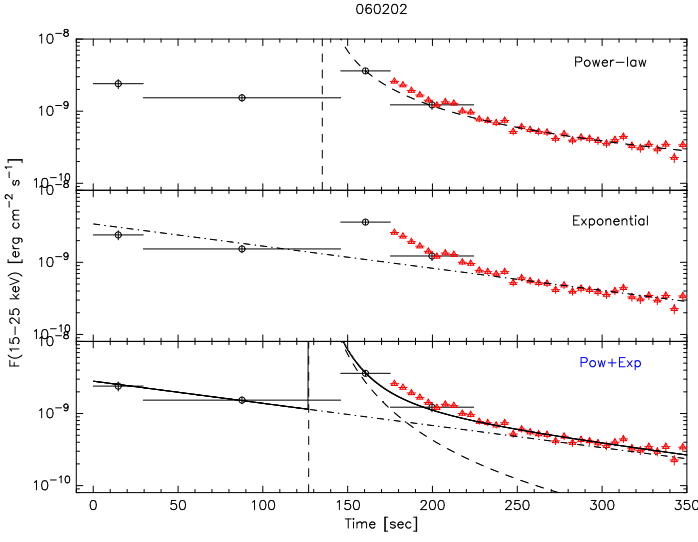


Fig. 4.— continued.

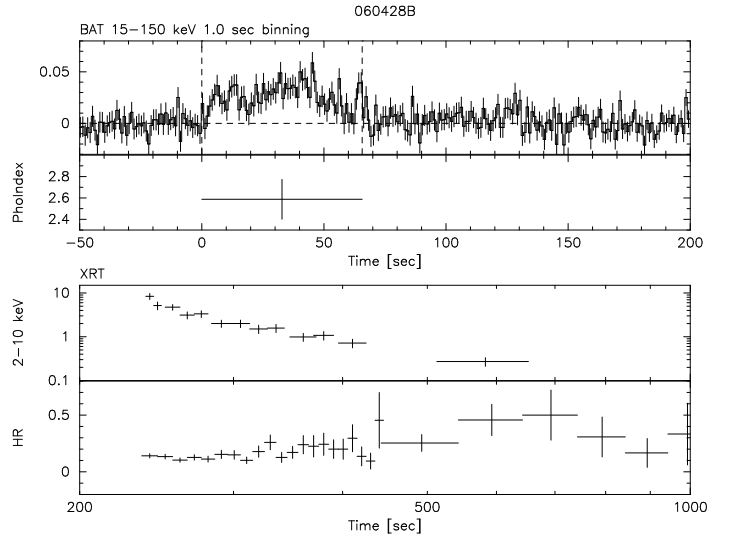
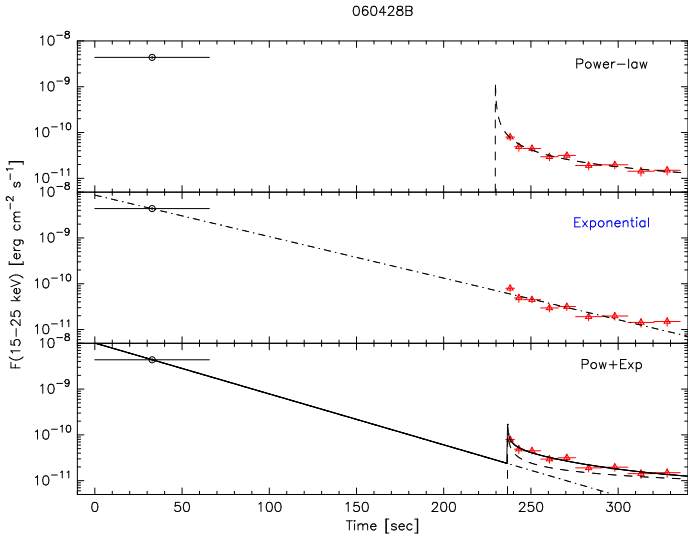
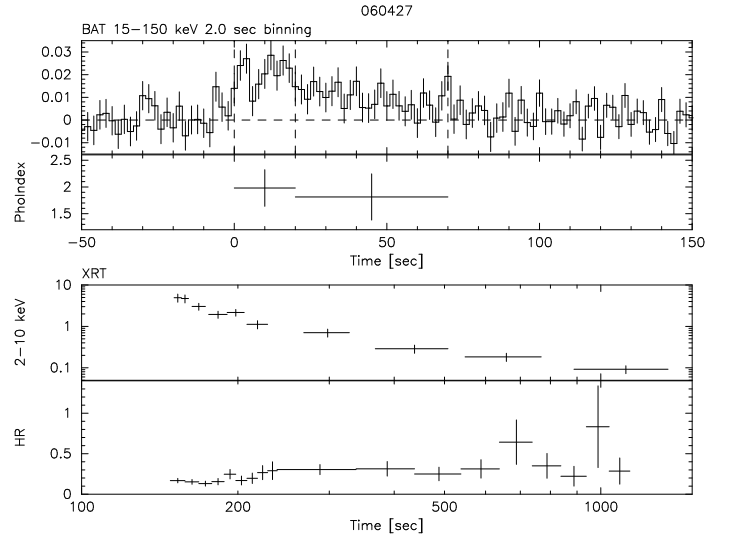
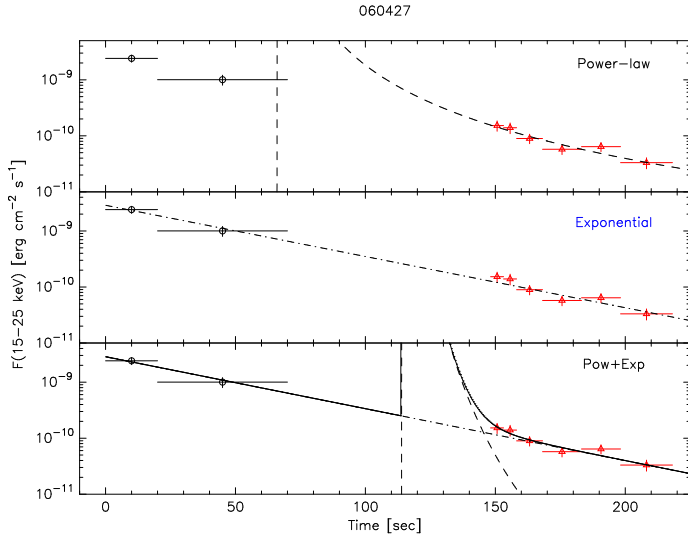
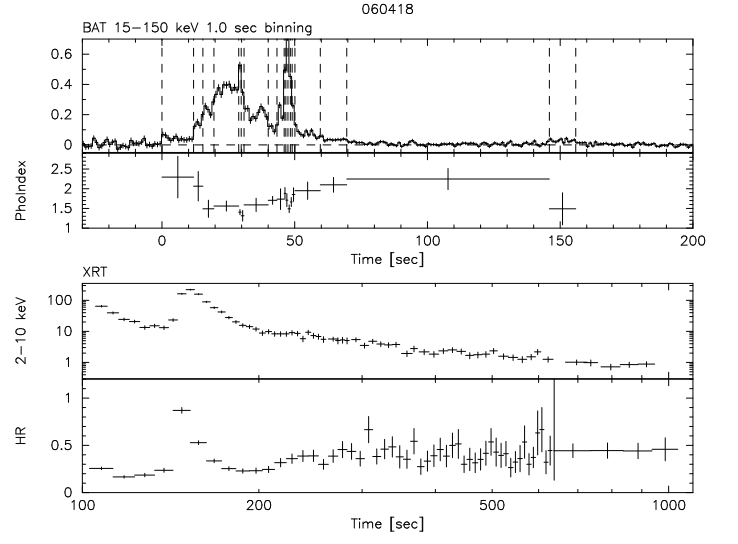
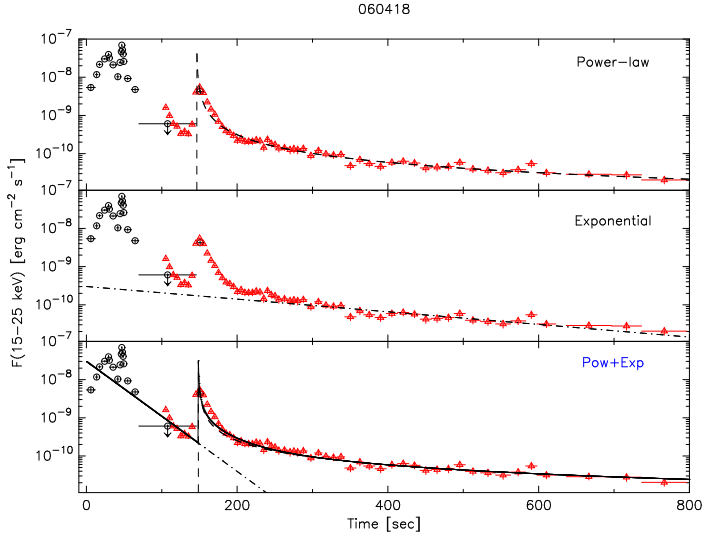


Fig. 5.— continued.

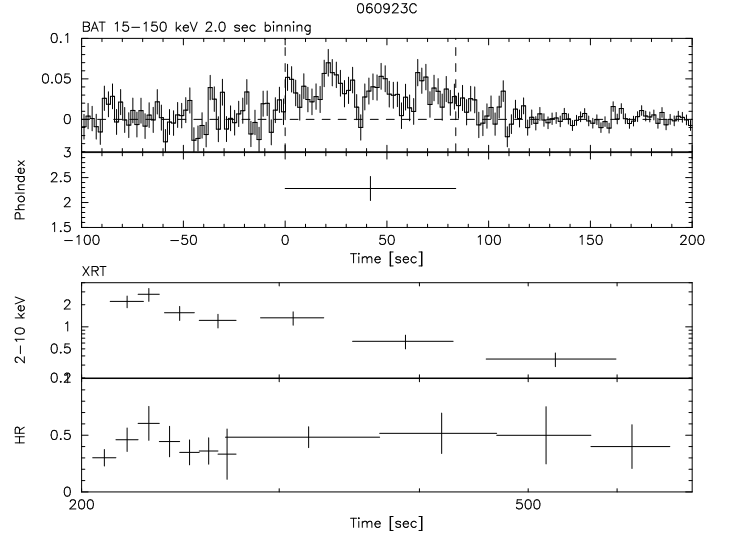
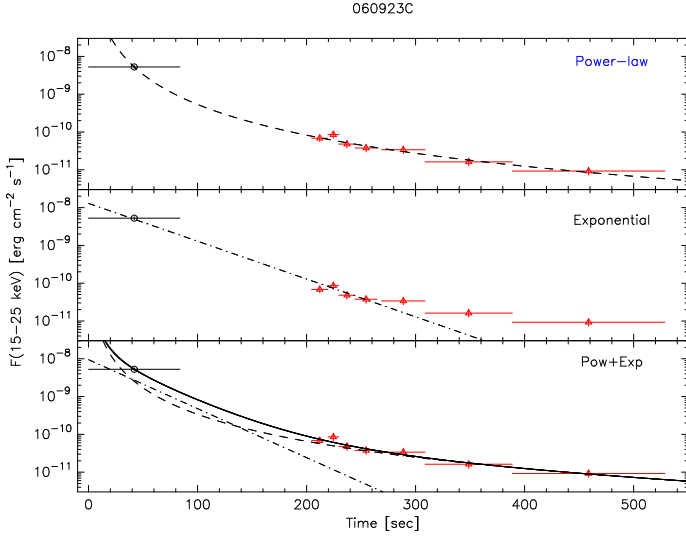


Fig. 6.— continued.

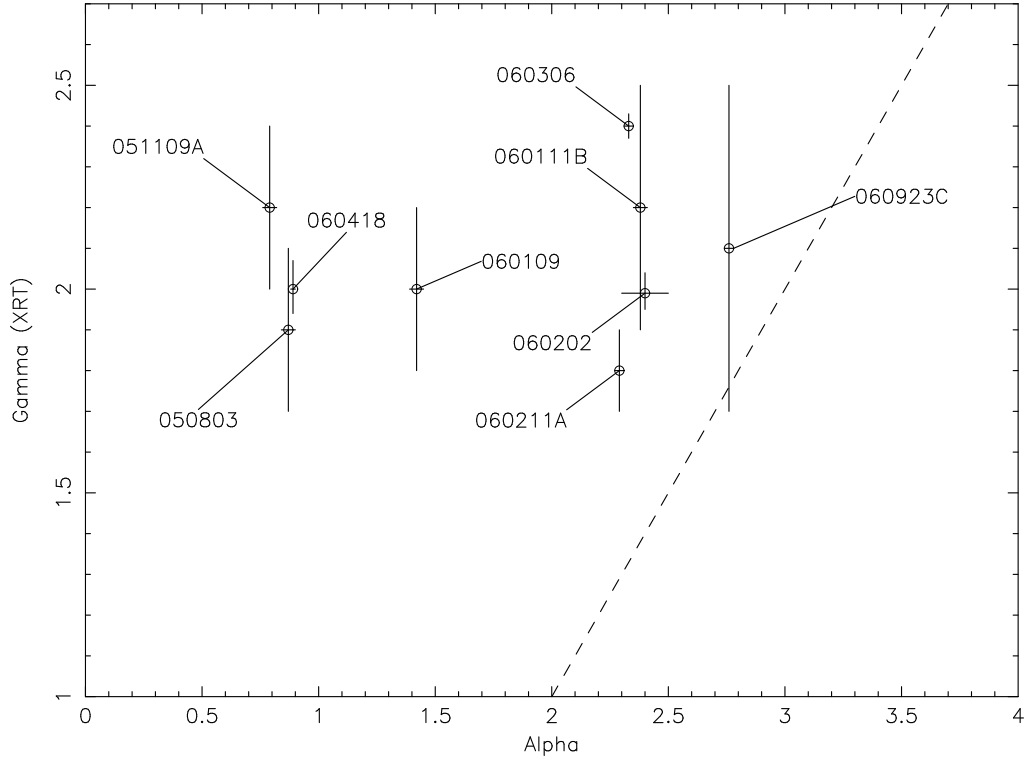


Fig. 7.— The relationship between the power-law decay index, α , of the best-fit light curve with a PLO component and a photon index, Γ_{XRT} . The dashed line is the expected relationship from the curvature effect ($\alpha = 1 + \Gamma_{XRT}$).

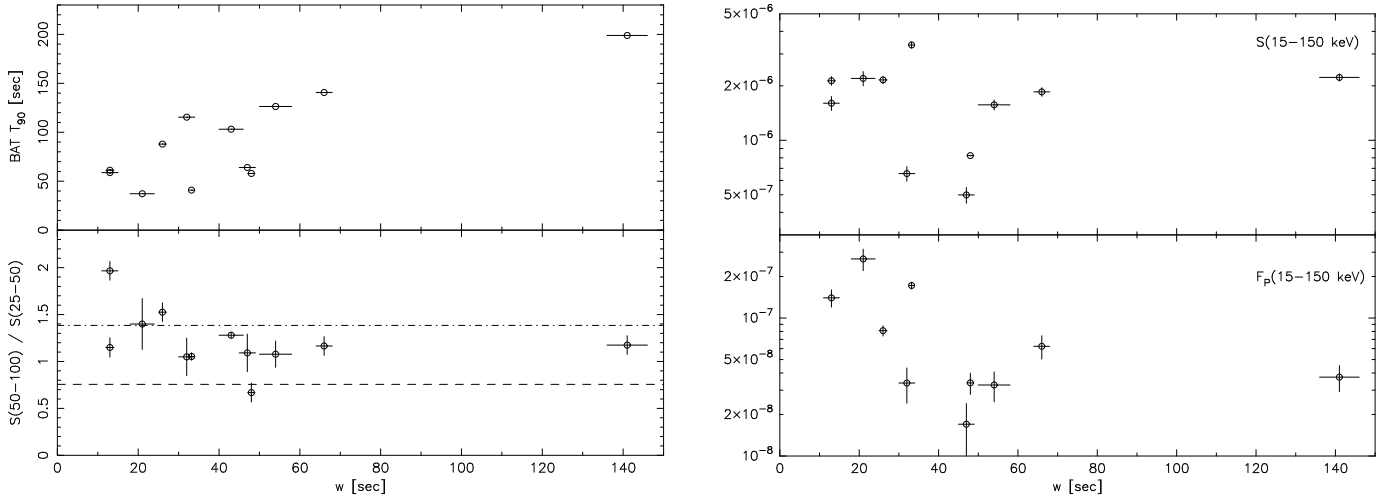


Fig. 8.— The relationship between the decay constant, w , of the exponential model and the BAT prompt emission properties. Top left: w vs. BAT T_{90} , Bottom left: w vs. the fluence ratio between the 50-100 keV and 25-50 keV band (the dotted and dash-dotted lines are the calculation assuming $E_{\text{peak}} = 30$ keV and $E_{\text{peak}} = 100$ keV, respectively, with a low and a high energy photon index of 1 and 2.5 in the Band function), Top right: w vs. the fluence in the 15-150 keV band, Bottom right: w vs. the 1-s peak flux in the 15-150 keV band.

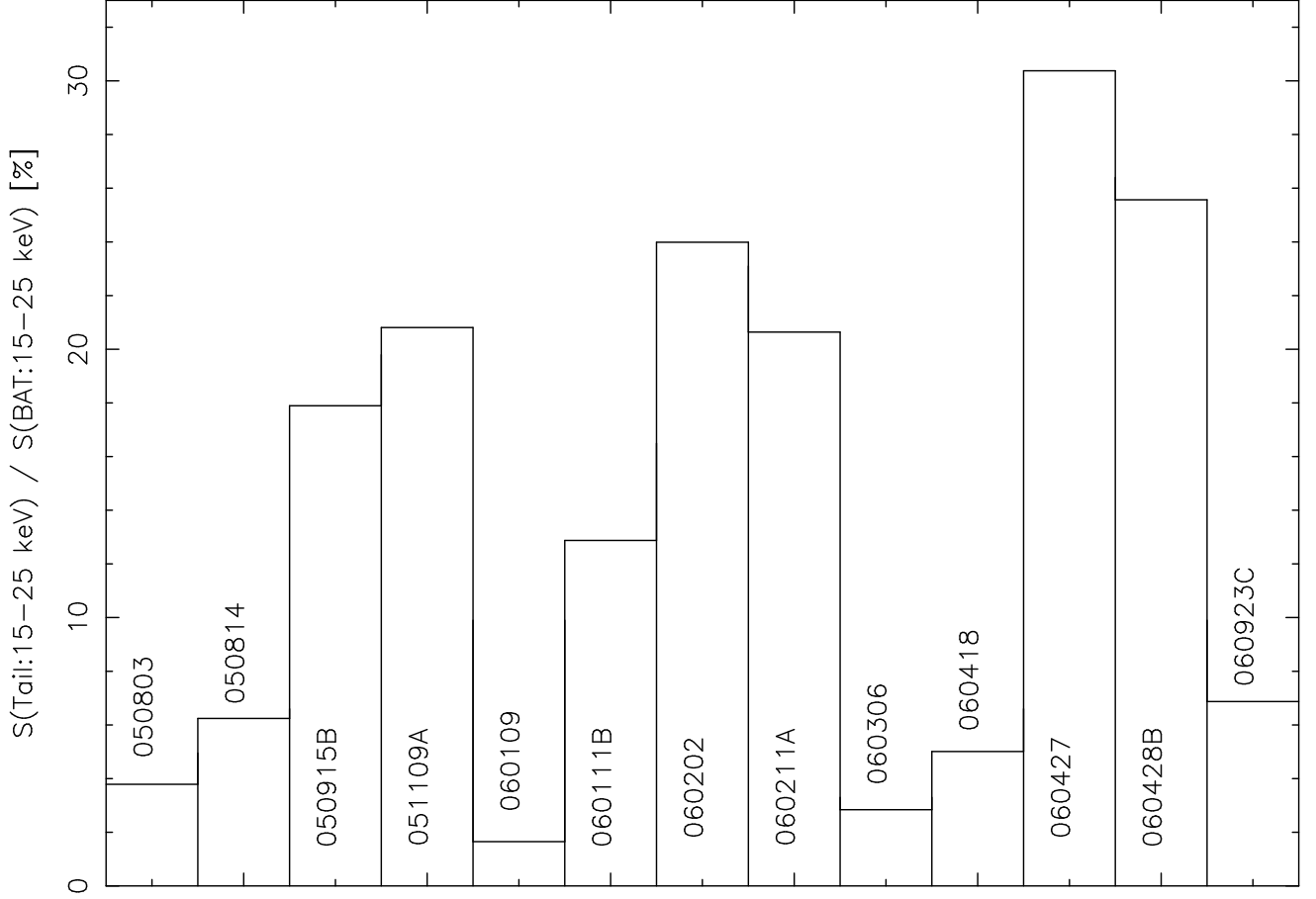


Fig. 9.— A histogram of the ratio, in percent, between the fluence accumulated from the end of the emission as detected by the BAT to 1000 s after t_0 ($S(\text{Tail:15-25 keV})$) and the fluence recorded by the BAT ($S(\text{BAT:15-25 keV})$).

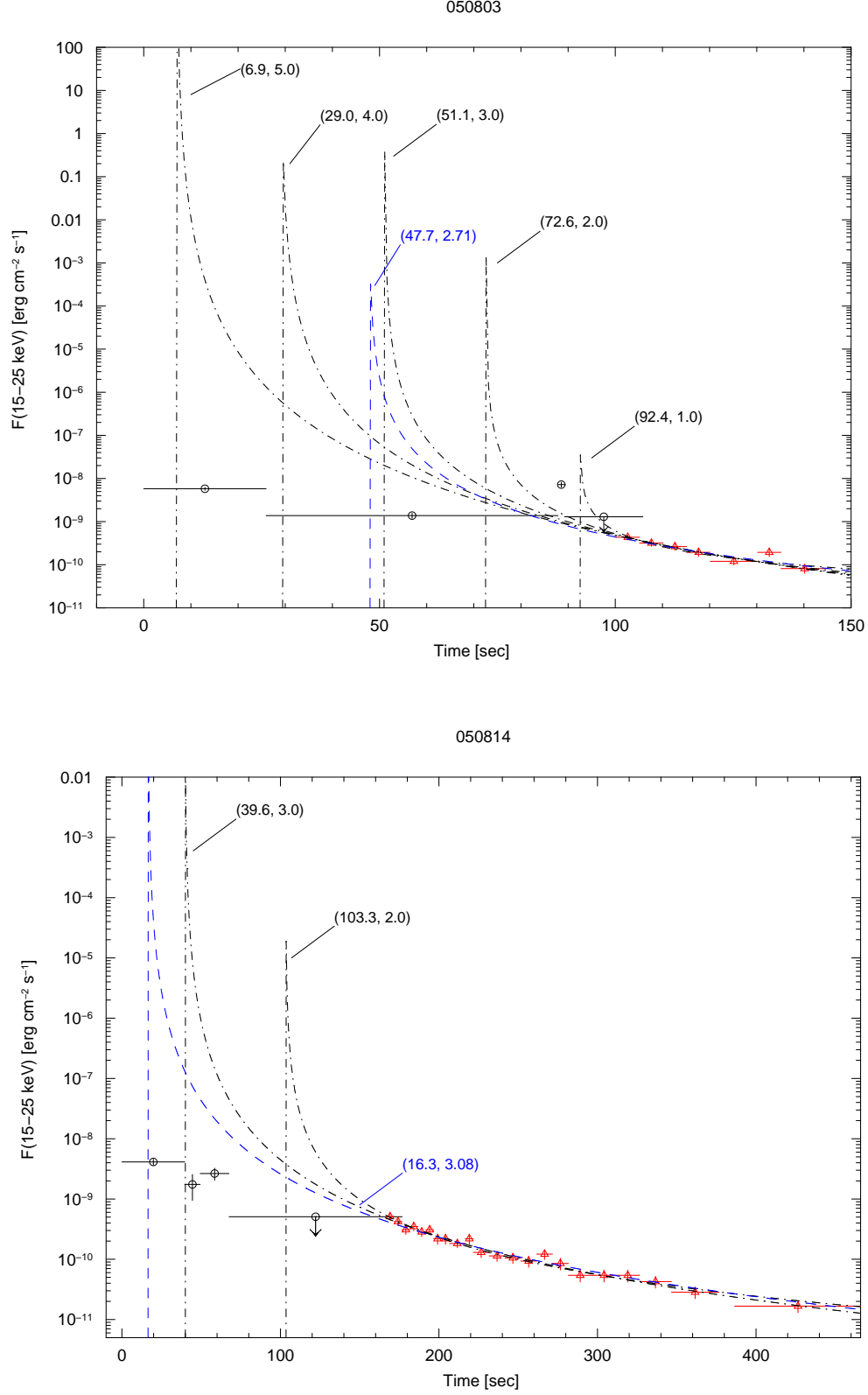


Fig. 10.— The BAT and XRT composite light curves of GRB 050803 (top) and GRB 050814 (bottom) overlaid with the best-fit PLO model for different choices of α and t_0^{pow} . The labels in the parentheses are (t_0^{pow}, α) . The model which represents Liang et al. (2006) is shown with a blue dashed line.